Time-Resolved Penetration Into Pre-Damaged, In-Situ Comminuted, and Compacted Powder Silicon Carbide

Charles E. Anderson, Jr.
Thilo Behner
Dennis L. Orphal
Arthur E. Nicholls
Volker Hohler
Matthias Wickert

Contract: W56HZV-06-C-0194

SwRI Report 18.12544/001

Prepared for

U.S. Army RDECOM-TARDEC
AMSRD-TAR-R
Warren, MI 48397-5000

October 2007

REPORT DOCUMENTATION PAGE

Form Approved
OMB No. 0704-0188

PLEASE DO NOT RETURN YOUR FORM TO THE ABOVE ADDRESS.

1. REPORT DATE *(DD-MM-YYYY)*	2. REPORT TYPE	3. DATES COVERED *(From - To)*
31-10-2007	Technical	07/21/2006 – 10/31/2007

TITLE AND SUBTITLE

Time-Resolved Penetration Into Pre-Damaged, *In-Situ* Comminuted, and Compacted Powder Silicon Carbide

5a. CONTRACT NUMBER
W56HZV-06-C-0194

5b. GRANT NUMBER

5c. PROGRAM ELEMENT NUMBER

6. AUTHOR(S)

Charles E. Anderson, Jr.[1], Thilo Behner[2], Dennis L. Orphal[3], Arthur E. Nicholls[1], Volker Hohler[2] and Matthias Wickert[2]

5d. PROJECT NUMBER
18.12544

5e. TASK NUMBER

5f. WORK UNIT NUMBER

7. PERFORMING ORGANIZATION NAME(S) AND ADDRESS(ES)

[1]Southwest Research Institute	[2]Fraunhofer Institute Kurzzeitdynamik	[3]International Research Assoc.
6220 Culebra Road	Ernst-Mach-Institute	4450 Black Ave., Suite E
San Antonio, TX 78238-5166	Eckerstr. 4, 79104 Freiburg	Pleasanton, CA 94566
United States	Germany	United States

8. PERFORMING ORGANIZATION REPORT NUMBER
12544/001

9. SPONSORING/MONITORING AGENCY NAME(S) AND ADDRESS(ES)

U.S. Army RDECOM-TARDEC
AMSRD-TAR-R
Warren, MI 48397-5000

10. SPONSOR/MONITOR'S ACRONYM(S)

11. SPONSORING/MONITORING AGENCY REPORT NUMBER

12. DISTRIBUTION AVAILABILITY STATEMENT

Approved for Public Release, Unlimited Distribution

13. SUPPLEMENTARY NOTES

The view, opinions, and/or findings contained in this report are those of the authors and should not be construed as an official Department of the Army position, policy, or decision, unless so designated by other documentation.

14. ABSTRACT

We have conducted a series of experiments to examine projectile penetration of cylindrical silicon carbide (SiC) ceramic targets that are pre-damaged to varying degrees under controlled laboratory conditions prior to ballistic testing. SiC was thermally shocked to introduce non-contiguous cracks. Another set of targets was thermally shocked and then additional damage was induced by load-unload cycling in an MTS machine while the ceramic specimen was confined in a 7075-T6 aluminum sleeve. Finally, targets were made by compacting SiC powder into a 7075-T6 aluminum sleeve. For each of these target types, long gold rod penetration was measured as a function of impact velocity v_p over the approximate range of 1 – 3 km/s, with most data between 1.5 and 3 km/s. Penetration as a function of time was measured using multiple independently timed flash X-rays. Results are compared to previous results for non-damaged (intact) SiC targets. Key results from these experiments include the following: 1) penetration is nominally steady state for $v_p > 1.5$ km/s; 2) for all target types, the penetration velocity u is a linear function of v_p, (except for the lowest impact velocities); and 3) it is found that $u_{\text{intact}} < u_{\text{pre-damaged}} < u_{\text{in-situ comminuted}} < u_{\text{powder}} < u_{\text{hydrodynamic}}$.

15. SUBJECT TERMS

silicon carbide, time-resolved penetration, penetration velocity, in-situ comminution, pre-damage, compacted powder

16. SECURITY CLASSIFICATION OF: UNCLASSIFIED			17. LIMITATION OF ABSTRACT	18. NUMBER OF PAGES	19a. NAME OF RESPONSIBLE PERSON
a. REPORT	b. ABSTRACT	c. THIS PAGE	None	47	Dr. Douglas Templeton
Unclassified	Unclassified	Unclassified			19b. TELEPONE NUMBER (*Include area code*) 586-574-5325

Table of Contents

List of Figures

List of Figures (Cont'd)

List of Tables

1.0 Introduction

There is now substantial evidence that when a projectile penetrates a semi-infinite brittle material, such as glass or ceramic, the projectile penetrates material that is damaged and weaker than prior to impact, e.g., Ref. [1]. It has been very difficult to obtain independent laboratory measurements of the constitutive parameters for failed ceramics because they are so strong. The initial estimate for the strength of failed silicon carbide (SiC) used by Holmquist and Johnson [2] was based on some experiments by Klopp and Shockey [3]. Subsequently, the strength of the failed surface was modified in order to match ballistic data [4]. However, determination of these computational constitutive properties for failed material has not been independent of improvements to numerical algorithms, e.g., [5-7]. Independently, work has been on-going to develop experimental procedures for laboratory characterization of *in-situ* failed ceramic and glasses [8-12]. Nevertheless, there have been various interpretations of exactly what these laboratory characterization data really imply.

Therefore, it was decided that a series of experiments to measure the penetration performance of a ceramic material with *initially* different strengths would be of value for the study and development of computational ceramic constitutive models. As a point of departure, experiments had been conducted that provide a fundamental set of well-defined data over a large range of impact velocities [13]. These experiments consisted of long-rod gold projectiles into intact SiC-N targets at impact velocities, v_p, from 2.0 to 6.2 km/s. The depth of penetration was measured as a function of time. As shown in Ref. [13], the penetration-time data are very linear; the slope of the data gave the penetration velocity, u. Statistical analysis of the data gave:

$$u = -0.5844 + 0.7547\ v_p \qquad (1)$$

with u and v_p in km/s. This linear least squares fit has an r^2 value of 0.999 and a root mean square error of 0.0371, i.e. 37 m/s.

Unlike glass, where a failure front can be clearly observed in experiments such as described in [1], SiC is optically opaque and no indirect evidence of a failure front was seen in the velocity range examined [13]. However, Dandekar [14] interpreted his data from combined pressure-shear experiments to show that the failure front for SiC has a velocity 6.5 ± 0.2 km/s, which is consistent with the findings in Ref. [13]. There, the maximum penetration velocity, by Eqn. (1), is 4.09 km/s; thus, it is reasonable to assume that the projectile penetrates failed material since the failure front propagates at a speed greater than the penetration velocity.[1]

This article documents the experimental results of a test series with cylindrical SiC-N ceramic targets with three different grades or degrees of damage: 1) thermally shocked but seemingly intact SiC-N; 2) thermally shocked SiC-N with additional mechanical (MTS) loading cycles to further damage the ceramic (*in-situ* comminuted); and 3) compacted SiC-N powder[2]. The powder, which has a grain size of ~1-3 μm, was selected since it represents the weakest state of failed SiC that we could imagine; i.e., we think the penetration response of the powdered SiC represents a lower limit for the strength of failed SiC. These variously damaged ceramics, contained in an Al-sleeve, were launched in the reverse ballistic mode against stationary gold

[1] This observation does not provide any indication of the lateral extent of failure.

[2] Compacted powder is not a pre-damaged ceramic; it is the raw material from which the intact SiC is fabricated. But for purposes of this article, we will use the word "damage" to describe all three specimen types.

rods. Impact velocities ranged from 1 to 3 km/s. Penetration of the gold rod was monitored with 5 flash X-ray tubes.

2.0 Experimental Set-Up

The investigated ceramic was SiC-N from Cercom, Inc. (density ρ_t = 3.2 g/cm^3) with a diameter of 18 mm and a length of 35 mm, placed inside a 7075-T6 aluminum sleeve of 31.5-mm outer diameter and 45-mm length (Fig. 1). The base plate was machined with a 45-deg cut, and then welded to the cylindrical sleeve.[3] After the specimen was prepared/inserted, a cover plate was press-fit into place using superglue.

Three specimen types were prepared:

- Thermally shocked (PD): pre-damage, in the form of non-contiguous cracks, was induced by heating the specimen for one hour at 750°C with a subsequent ice water quench (3 cycles); thereafter, placing in the Al-sleeve. Although cracked, the specimens have integrity and strength [8].
- *In-situ* comminuted (C): specimen thermally shocked as above and then subjected to six loading/unloading cycles to 1.7 GPa while in the aluminum sleeve. The loading was done using a MTS machine. After the cyclic loading, the loading anvils were removed and the cover and base plates were applied. (The specimen, if removed from the aluminum sleeve, has interlocked comminuted pieces, which crumbles easily under a very small—"finger-pressure"—applied load.)
- Compacted powder (CP): SiC-N powder was placed into the Al-sleeve through a series of incremental pours and compaction using an MTS machine, achieving 72-73 % of the theoretical density of SiC-N ($\rho_{\text{comp.powder}} \approx 2.35$ g/cm^3).

The rods were made of pure gold (99.99%) and had a diameter of 1 mm and a length of 70 mm with the following material properties: density ρ_p = 19.3 g/cm^3; hardness 65 HV5; UTS 220 MPa and elongation 30%.

The reverse ballistic method was used in conducting the experiments. The penetration process was observed with five 180 kV flash X-rays. Figure 2 shows the arrangement for the impact tank together with the positioning of the X-ray heads used to image the penetration process. The tests were performed with a two-stage light-gas gun, using a separating sabot to launch the targets (a non-separating sabot was used for the first few experiments but abandoned later to better control yaw).

[3] Simulations by T. Holmquist [15] indicated that the base plug could possibly move due to pressure from the penetrating rod. As the base aluminum/ceramic interface is used as a spatial fiducial for measurements, it was unacceptable for this "line" to move relative to the sleeve. Therefore, the base plug was welded into place. Simulations indicated that the weld would be sufficient to keep the base plug and cylinder firmly attached.

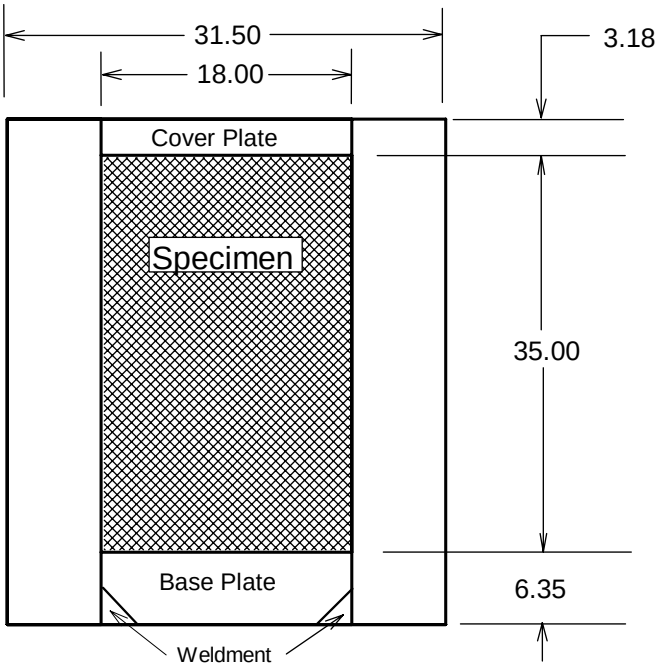

Figure 1. Test specimen (dimensions mm).

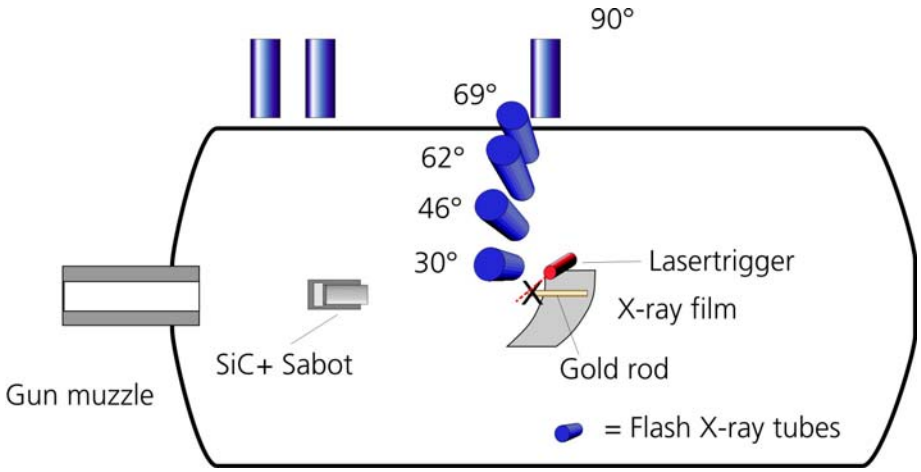

Figure 2. Test set-up.

The time measurements for the flash X-ray shadowgraphs are very accurate (to better than ±5 ns). Thus, the error for the velocities determined from the X-ray shadowgraphs rest in the accuracy of the position measurement, which is about ± 0.1 to 0.15 mm.

To reduce weight of the sabot package in order to achieve higher impact velocities, the diameter of the Al-sleeve was machined to 26 mm for v_p > 2 km/s. Results showed no influence from the reduced diameter.

3.0 Results and Analysis

3.1 Position-Time Data

An example of the flash radiographs is shown in Fig. 3, which is for experiment 11066, one of the *in-situ* comminuted specimens. Time zero is measured from impact on the aluminum cover plate. Position is measured from the beginning of the ceramic specimen; thus, the initial impact location is –3.18 mm since the cover plate has a thickness of 3.18 mm. The position-time data for all the experiments are shown in Figs. 4 through 6. A complete tabulation of the position-time data for the 23 experiments is given in Appendix A. Copies of the flash X-ray shadowgraphs are shown in Appendix B.

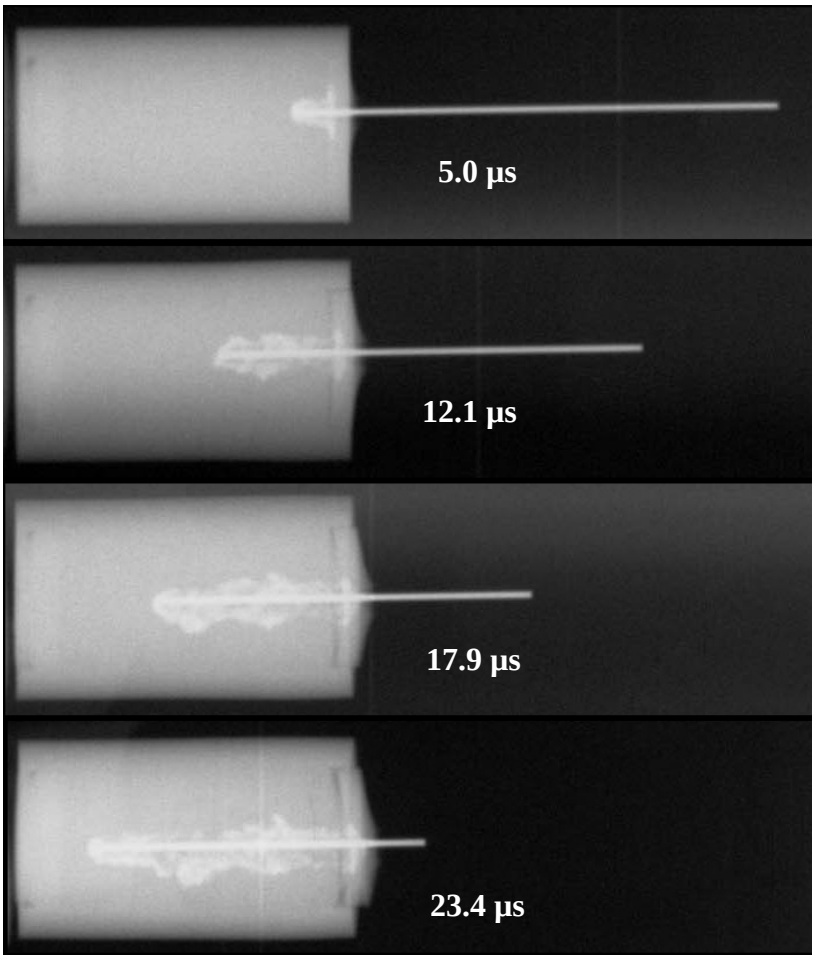

Figure 3. Flash radiographs of Expt. 11066, v_p = 2.585 km/s.

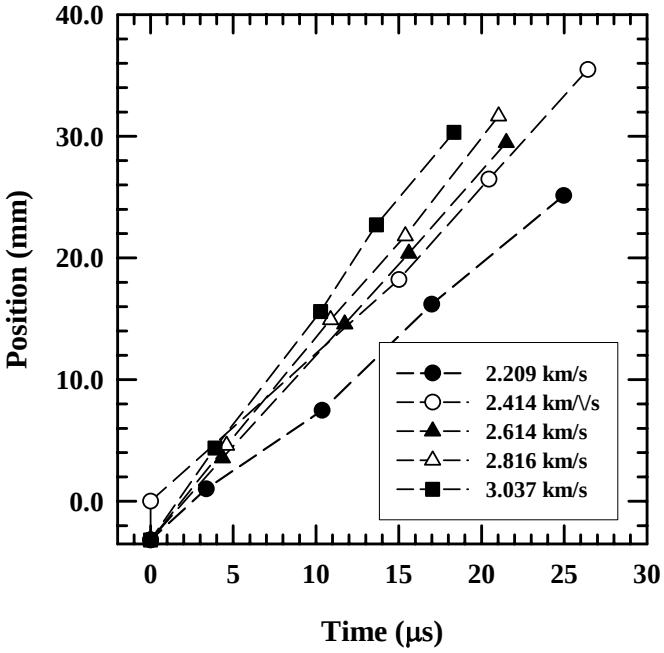

Figure 4. Position vs. time data for thermally pre-damaged specimens.

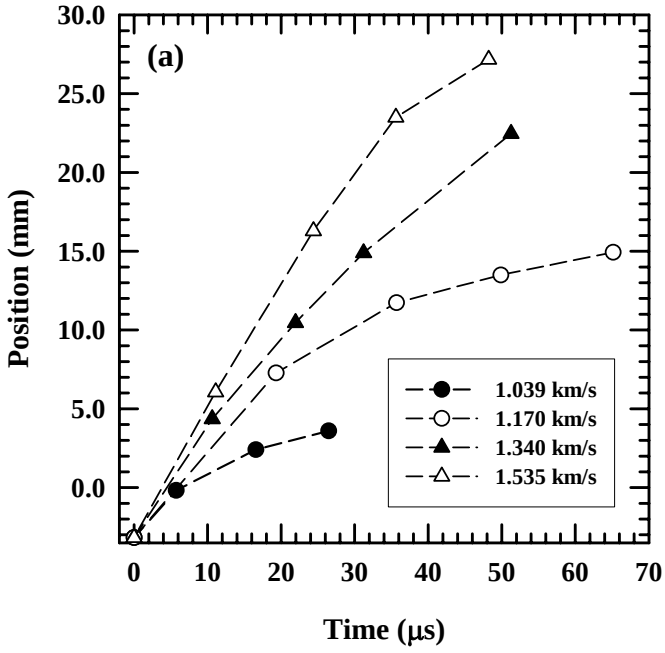

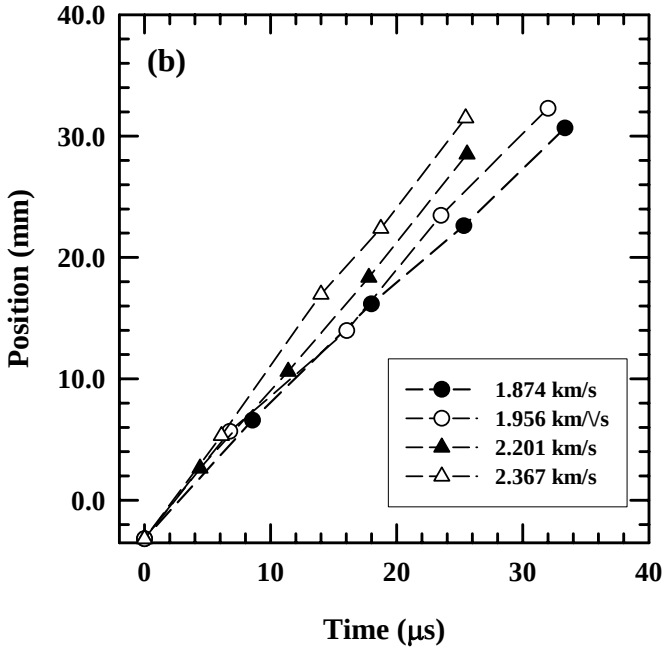

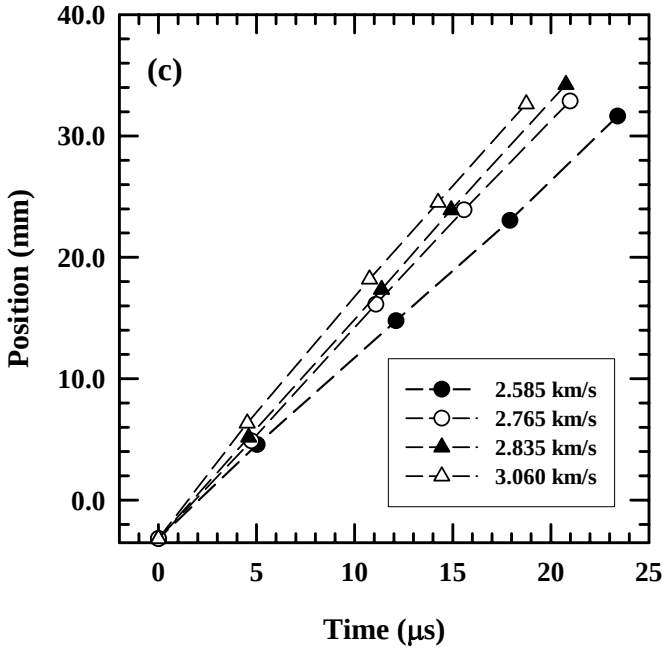

Figure 5. Position-time data for *in-situ* damaged specimens.

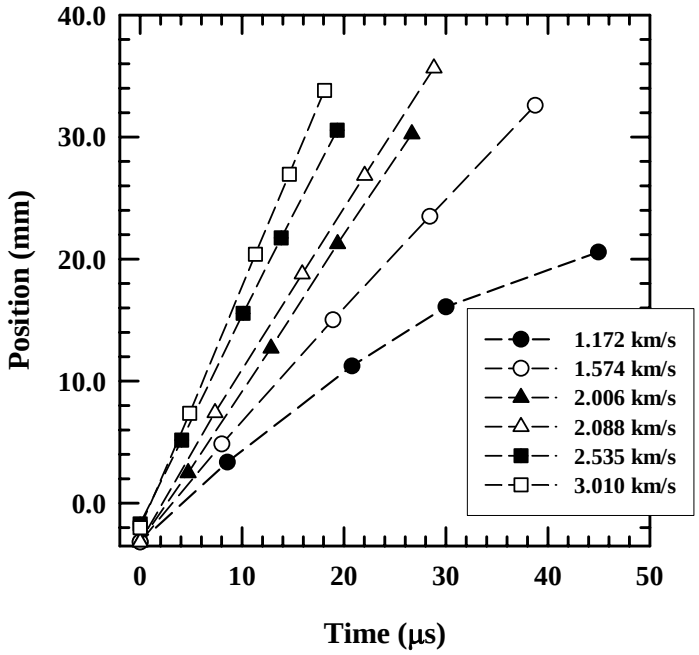

Figure 6. Position vs. time data for compacted powder specimens.

3.2 Analysis of Experimental Data

The position-time and rod length-time data are quite linear for most experiments. Steady-state penetration for the complete penetration phase was observed for impact velocities above 1.8 km/s for the *in-situ* comminuted ceramic, Fig. 5; and above 1.5 km/s for the compacted powder specimens, Fig. 6. The thermally shocked targets, Fig. 4, were launched at higher velocities; all of these had steady-state penetration.

It is instructive to examine some of the flash radiographs for tests exhibiting nonlinear penetration rates. The following examples are all for *in-situ* damaged specimens. The rod penetrated only a few millimeters in Expt. 11046 (v_p = 1.039 km/s). It can be seen in Fig. 7 that there is large radial flow of the Au rod material. At a slightly higher impact velocity, Fig. 8 (v_p = 1.170 km/s), there is not as much radial flow of rod material as in Fig. 7, but the penetration crater diameter remains quite large (as compared to the more typical penetration channel, Fig. 3). In Fig. 9 (v_p = 1.535 km/s), the early-time penetration channel profiles appear typical, but in the last flash X-ray (48.2 μs), it is evident that there was a large increase in penetration channel diameter, implying substantial radial flow at late time. A possible explanation for the observed phenomena is provided below.

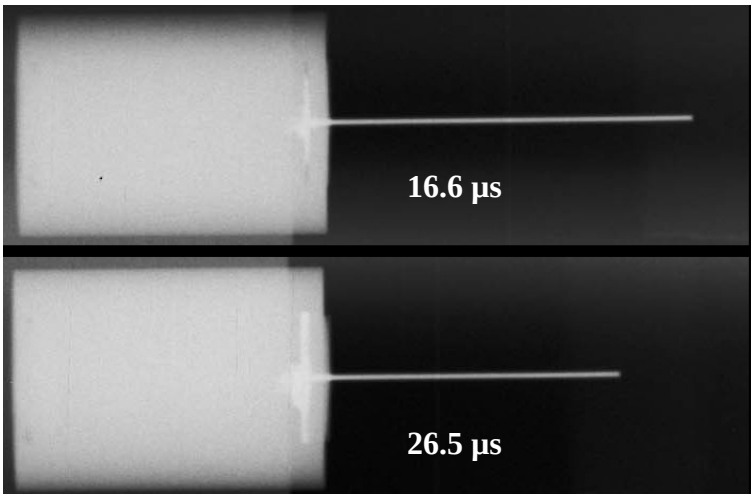

Figure 7. X-ray shadowgraphs for Expt. 11046: *in-situ* comminuted specimen, v_p = 1.039 km/s.

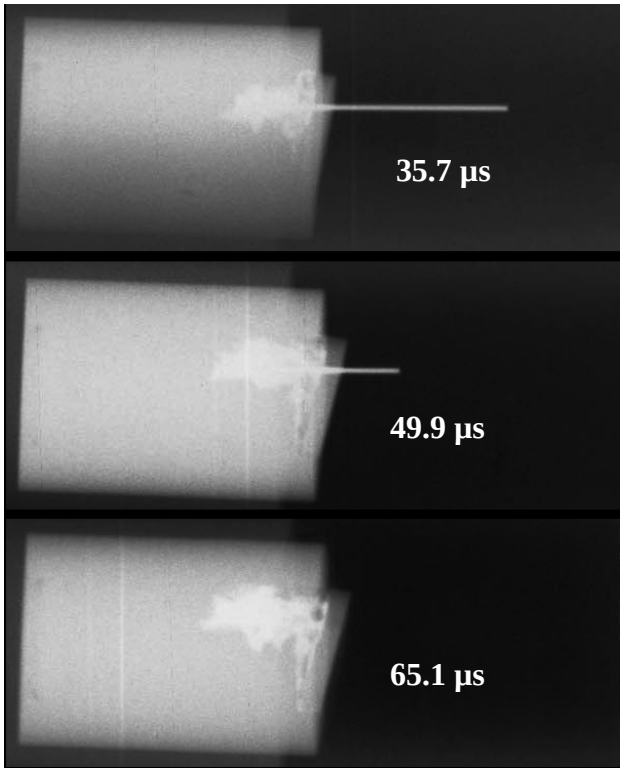

Figure 8. X-ray shadowgraphs for Expt. 11048: *in-situ* comminuted specimen, v_p = 1.170 km/s.

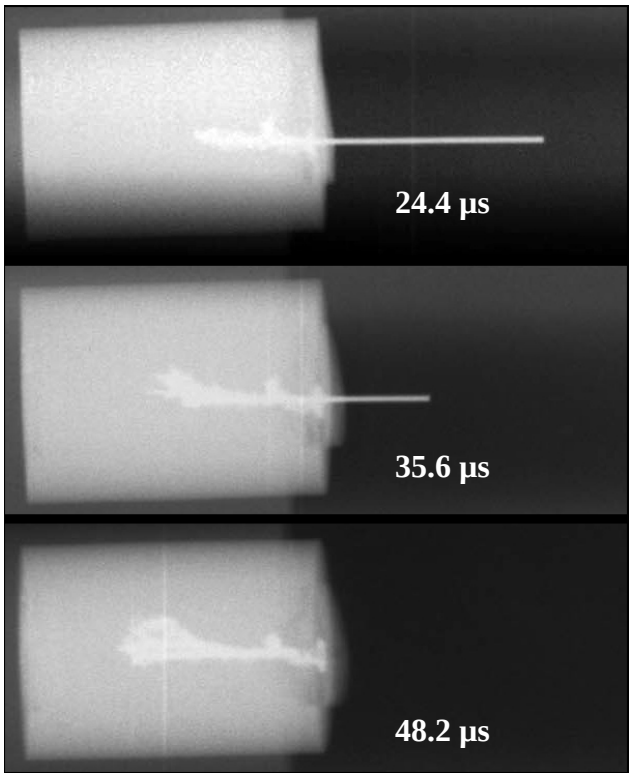

Figure 9. X-ray shadowgraphs for Expt. 11052: *in-situ* comminuted specimen, v_p = 1.535 km/s.

Penetration velocity u and consumption velocity v_c were calculated by a linear regression of the position of the rod inside the ceramic and the length of the remaining rod versus time after impact. The slopes of these regression fits provide the u and v_c, respectively. The position-time data measured from the X-ray shadowgraph shown in Fig. 3 (Expt. 11066, v_p = 2.585 km/s) are plotted in Fig. 10 as the solid circles. The long dashed line in Fig. 10 denotes the regression result for the position-time data. The penetration velocity for this experiment is 1.467 km/s; the correlation coefficient, r^2, is 0.9996.[4]

As already discussed, position-time data for the lower velocity experiments exhibit some nonlinearity. The analysis procedure for these experiments is a little different than for the experiments that show linearity over the entire X-ray data set. For example, the data for Expt. 11052, v_p = 1.535 km/s are also plotted in Fig. 10. Here, the position-time data, indicated by the open triangles, show a linear behavior for most of the penetration within the ceramic, but penetration no longer continues linearly with time for the last X-ray. Consequently, calculations of u (and v_c) from those low v_p experiments were done with only the linear penetration phase, which is denoted by the short dashed line in Fig. 10. Using this procedure, a penetration velocity of 0.713 km/s is calculated for Expt. 11052 with a very good correlation coefficient. The other low-velocity experiments were done similarly.

[4] There is no requirement for the linear regression to pass through the impact point (the front cover plate) at t = 0 since the penetration velocity through the aluminum cover plate does not equal that within the specimen.

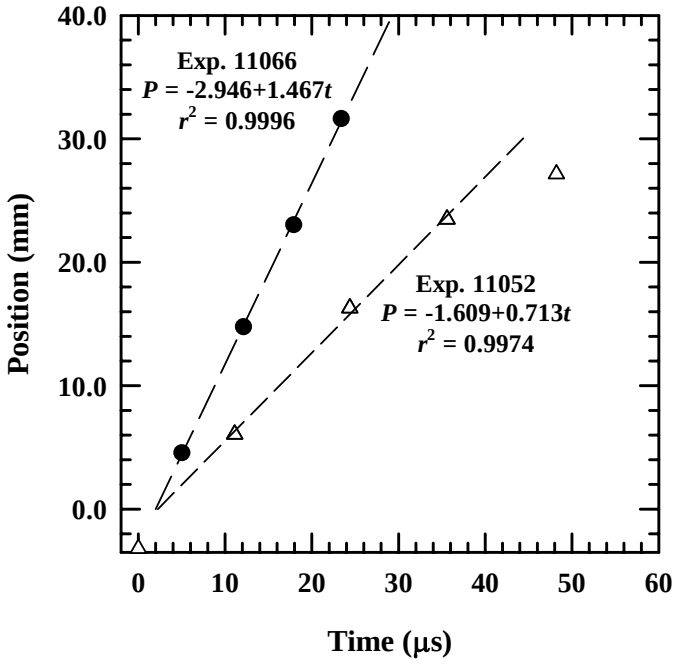

Figure 10. Determination of penetration velocity *u* for two experiments: Expts. 11066 (v_p = 2.585 km/s) and 11052 (v_p = 1.535 km/s).

Due to the inhomogeneous nature of the pre-damaged and *in-situ* comminuted ceramic specimens (randomly distributed cracks and consequently some flow of rod material into those cracks), small inconsistencies can occur for the position-time data even at higher v_p so that the linearity of the data can be "disturbed." An example is shown in Fig. 11 for Expt. 11056 at v_p = 1.956 km/s.

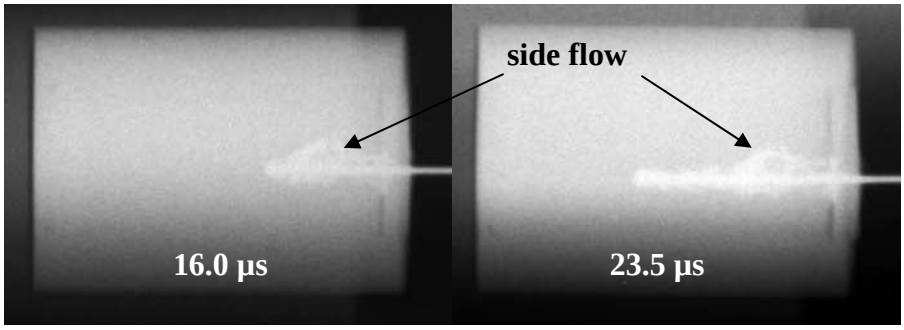

Figure 11. Flow of rod material in a crack(s), Expt. 11056.

We have determined the average penetration velocity and consumption velocity for each of the 23 experiments using least-squares linear regression. As described above for Expt. 11052, only the linear region of the data is included in the analysis for the low velocity experiments. The results for the 3 different types of SiC specimens (PD, C, and CP) are summarized in Table 1. Test results are sorted by increasing impact velocity v_p for each target type. The results are plotted in Fig. 12. The solid data points denote the data that have only linear position versus time response, while the open symbols denote lower v_p data that have significant non-linearity in their position-time behavior.

Table 1. Experimental Results

Exp	Target	yaw [°]	oc [mm]	v_p [km/s]	u [km/s]	v_c [km/s]	R_t [GPa]
11065	PD7	2.5	1.8	2.209±0.010	1.135±0.050	1.058±0.063	8.7
11068	PD4	1.2	3.7	2.414	1.511±0.004	0.871±0.033	3.7
11069	PD5	1.8	2.7	2.614±0.007	1.510±0.009.	1.1070.021	8.2
11071	PD6	1.4	3.8	2.816±0.003	1.638±0.028	1.161±0.036	8.7
11074	PD8	4.7	2.1	3.037±0.009	1.816±0..52	1.190±0.022	8.4
11046	C9	-	-	1.039±0.003	0.120	0.951	8.7
11048	C10	2.0	4.7	1.170±0.007	0.272	0.918	8.0
11050	C11	4.5	3.4	1.340±0.002	0.514±0.018	0.853±0.055	6.6
11052	C12	2.1	3.1	1.535±0.010	0.713±0.036	0.845±0.035	6.1
11058	C16	1.2	4.0	1.874±0.007	0.965±0.018	0.923±0.024	6.7
11056	C13	1.7	2.6	1.956±0.006	1.071±0.049	0.884±0.052	5.7
11064	C15	0.9	0.0	2.201±0.005	1.222±0.027	0.999±0.025	7.2
11076	C20	4.0	2.9	2.367±0.007	1.340±0.043	1.018±0.037	7.1
11066	C17	0.6	2.3	2.585±0.001	1.467±0.022	1.105±0.034	8.3
11070	C18	0.6	6.0	2.765±0.005	1.725±0.020	1.037±0.012	5.6
11075	C19	1.6	3.9	2.835±0.004	1.801±0.010	1.001±0.014	4.5
11072	C14	4.7	2.5	3.060±0.007	1.849±0.020	1.180±0.014	8.0
11049	CP1	0.9	1.8	1.172±0.004	0.596±0.033	0.593±0.043	3.0
11053	CP2	3.1	5.4	1.574±0.006	0.902±0.009	0.676±0.008	3.5
11057*	CP3	2.2	9.5	2.006±0.006	1.269±0.009	0.765±0.010	3.8
11077	CP6	2.3	1.2	2.088±0.004	1.315±0.006	0.770±0.009	2.9
11067	CP5	0.2	1.2	2.535±0.004	1.663±0.021	0.877±0.007	4.2
11073	CP4	1.2	2.3	3.010±0.007	1.999±0.009	0.970±0.003	2.7

*: hit at the edge of ceramic-sleeve interface – probably not suitable for evaluation
oc: off-center hit

Target resistance R_t listed in Table 1 was calculated from the Tate equation [16]:

$$R_t - Y_p = \frac{1}{2}\rho_p\left(v_p - u\right)^2 - \frac{1}{2}\rho_t u^2 \qquad (2)$$

using the u and v_c values ($v_c \cong v_p - u$) from the Table, and with a penetrator strength $Y_p = 0$ since the gold is quite weak.

Returning to our observation concerning the nonlinear penetration-time response of the rod at the lower impact velocities, we note that as long as the ratio $u/(v_p - u) >> 1$, the penetration is linear with time, i.e., the rod penetrates with a steady-state velocity. For $u/(v_p - u) \le 1$, the overall position-time response is nonlinear, with a decreasing rate of penetration as time progresses. Physically, this implies that so long as the penetration rate is greater than the rate of rod consumption, penetration is linear. However, when rod consumption rate is greater than the penetration velocity, then the rod material "piles up" near the rod/target interface and, since the rod material must go somewhere, there is radial growth of the penetration channel.

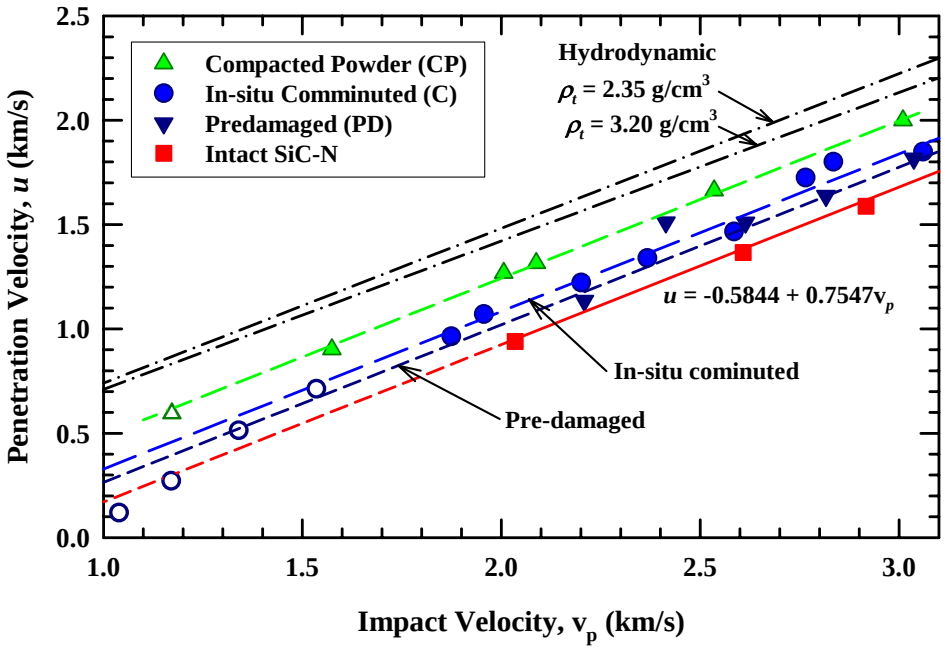

Figure 12. Penetration velocity u vs. impact velocity v_p for different types of SiC-N specimens.

3.3 Comparison of Penetration Rates

The test series with long-rod impact on intact SiC-N in [13] provided a linear relationship between penetration velocity u of the gold rod in the ceramic and impact velocity v_p as described by Eqn. (1). The regression line for the intact SiC has been extrapolated in Fig. 12 to lower impact velocities, as indicated by the dashed line. We know that the u versus v_p response of intact SiC-N cannot be linearly extrapolated to the very low impact velocities shown in Fig. 12 because at some impact velocity, the projectile begins to dwell at the target interface (for example, see [17]), but the linear extrapolation serves as a "trend" line.

The evaluations of u for the PD-, C- and CP-SiC ceramic specimens show a very similar behaviour. Linear regression analyses were performed on the experimental data and these detailed results are given in Appendix B. However, it is noted that the three sets of data for the damaged SiC are nominally parallel to the intact ceramic response line. Therefore, using the principal of Occam's razor (simple explanations should be preferred to more complex ones), linear regression analyses were conducted to determine the intercepts for the PD, C, and the CP data, *with the slope constrained to be 0.7547*, the value determined for the intact SiC data. The results are:

$$\text{Pre-damaged (PD):}\quad u = -0.4538 + 0.7547\, v_p \quad r^2 = 0.8885;\ RMS = 0.097 \text{ km/s} \qquad (3)$$

$$\textit{In-situ} \text{ comminuted (C):}\quad u = -0.4231 + 0.7547\, v_p \quad r^2 = 0.9788;\ RMS = 0.055 \text{ km/s} \qquad (4)$$

$$\text{Compacted powder (CP):}\quad u = -0.2629 + 0.7547\, v_p \quad r^2 = 0.9985;\ RMS = 0.019 \text{ km/s} \qquad (5)$$

where r^2 is the squared correlation coefficient between u and v_p, and *RMS* is the root mean square error associated with the residuals (i.e., the difference between the observed and predicted u values from the regression fit).

Of the three damaged materials, the PD regression fit, Eqn. (3), has the smallest squared correlation coefficient and largest standard deviation of the residuals, largely because the data point at 2.4 km/s deviates more than 6.5 standard deviations from a regression model fitted without the point. If this data point is removed, the regression fit becomes:

$$\text{Pre-damaged (mod):}\quad u = -0.4895 + 0.7547\, v_p \qquad r^2 = 0.9950;\ RMS = 0.037 \text{ km/s} \tag{3a}$$

Given this result, it can be concluded that the one point at 2.4 km/s appears to be an outlier, and that in general, the pre-damaged ceramic provides more penetration resistance than the *in-situ* comminuted ceramic. The resulting regression lines for the PD (using Eqn. 3a), C and CP materials are shown in Fig. 12. For comparison purposes, the hydrodynamic responses for solid density SiC-N (3.2 g/cm^3) and for the density of the compacted powder (2.35 g/cm^3) are also shown.

Examining the intercepts of Eqns. (3-5) and comparing them to the intercept for the initially intact material, Eqn. (1), it is noted that the penetration resistance (as measured by the penetration velocity) increases as the intercept becomes more negative. Thus, making the physically reasonable correlation between penetration velocity and some sort of average strength of the ceramic specimens, the order of increasing strength is compacted powder (weakest), *in-situ* comminuted, pre-damaged, and intact (strongest) ceramic. This, of course, is not surprising. Perhaps what is surprising is that the strength of compacted powder is considerably greater than a zero-strength (hydrodynamic) material, and that the strength of the *in-situ* comminuted ceramic is not greatly different than pre-damaged ceramic.

As noted, Eqns. (3-5) assume that the slope of all the u-v_p curves is 0.7547, the same as determined for the earlier experiments using intact SiC targets [13]. It is clear from a visual examination of Fig. 12 that constraining the u-v_p slope in this manner provides excellent fits to the damaged SiC data for all the tests exhibiting linear penetration-time behavior (i.e. steady-state penetration). As noted above, for completeness, Appendix C contains the results for the least-squares fits of the data for all the damaged SiC targets types when the u-v_p slope is not constrained. An examination of the regression coefficients in Appendix C shows that the unconstrained slopes of the linear u-v_p curves are not very different from the value of 0.7547 given the size of the *RMS*. There is a statistical test that addresses the question of whether the u-v_p slopes given in Appendix C differ significantly from the slope of 0.7547 of the intact SiC tests. The statistical analysis shows that the probability of the observed slopes for the three types of damaged SiC being different from 0.7547 is small. This result is far different than our expectations before performing these experiments.

3.4 Estimates for Drucker-Prager Constitutive Constants

Although it is preferable to obtain constitutive constants from independent laboratory experiments, the data from these ballistic experiments can be used to estimate constants assuming the form of the constitutive model. A Drucker-Prager model is typically used to express the response of pressure-dependent granular materials:

$$\sigma_{eq} = \min\left(A_o + \beta P,\ \bar{Y}\right)$$

where σ_{eq} is the equivalent stress, P is the pressure, and A_o, β, and $\overline{Y}$ are the three constants that need to be determined. $\overline{Y}$ is usually called the cap, and it limits that maximum shear stress that can be supported by the material. These constants were determined by requiring numerical simulations to match the penetration-velocity versus impact-velocity response. The higher impact velocity experiments provide an estimate for $\overline{Y}$, and the lower velocity experiments are used to determine the other two constants. The Drucker-Prager constants for the *in-situ* comminuted material are: A_o = 0.0455 GPa, β = 2.7, $\overline{Y}$ = 2.25 GPa. A two-parameter model, with only the constants A_o = 1.0 GPa, β = 0.5 fit the experimental data equally well, but we believe that such a large value for A_o is not physically realistic for the *in-situ* comminuted material. The details of obtaining these constitutive constants are found in [18].

Holmquist and Johnson [19] determined the constants for the compacted powder. Assumptions were made in determining the equation of state to account for compaction of the powder to fully dense SiC during the penetration process. They found for the compacted powder that a two-parameter model fit the data better than a three-parameter model. Model constants are: A_o = 0.13 GPa, β = 0.62. The authors also conducted sensitivity studies to quantify the effect of their assumptions; details are found in [19].

4.0 Summary and Conclusions

The penetration of a gold rod into pre-impact damaged SiC-N targets was measured. The SiC targets had three distinct levels or degrees of damage: 1) non-contiguous cracking as a result of thermal shocking the ceramic; 2) highly comminuted SiC as a result of six load-unload cycles after initial pre-damaging by the same thermal shock process; and 3) compressed powder at about 72-73% of the theoretical solid density. The results from the tests using these pre-impact damaged targets were compared to the results from essentially identical experiments using SiC-N targets that were intact prior to impact.

There are a number of important as well as surprising results from these pre-impact damaged experiments. Briefly these include:

1. Penetration in all three types of damaged SiC targets achieves steady-state velocity, u, for all but the lowest impact velocity experiments.
2. For all three levels of damage, u is a linear function of the impact velocity v_p. A statistical comparison of the least-squares regression analyses indicates that the slope of u versus v_p for the three types of damaged SiC targets are not significantly different from that for the initially intact SiC. Thus, the penetration velocities for both the pre-impact intact and all three types of damaged SiC targets can be written as $u = a + 0.7547v_p$ with a dependent upon the degree of damage (the linear u-v_p relationship does not apply to the lowest impact velocities, where nonlinearity is observed in the penetration-time response). This seems to imply, at least for these materials, that in the linear u-v_p relationship ($u = a + bv_p$), effects of target strength are largely contained in the intercept "a" [20].
3. Even for the targets that were only thermally shocked and exhibited non-contiguous cracking, there is a significant reduction in strength, as reflected in the penetration velocity, compared to the pre-impact intact material. In

fact, the response of the pre-damaged material is very similar to the *in-situ* comminuted material. This is surprising.

4. It is found that $u_{\text{intact}} < u_{\text{pre-damaged}} < u_{\text{in-situ comminuted}} < u_{\text{powder}} < u_{\text{hydrodynamic}}$, corresponding to a reduction in strength or resistance to penetration in the same order.

As discussed above, the data can be used to validate the constitutive constants A_o, β, and $\overline{Y}$ for the Drucker-Prager model for the *in-situ* comminuted and compacted SiC-N powder.

There is substantial evidence that for an initially (prior to impact) intact target, a rod actually penetrates material that has failed as a result of the impact shock and/or stresses associated with the penetration process itself, although the axial and radial extents of this failed region are unknown (except within the context of an assumed model). A key objective, and a major motivation of this effort, is to understand the physical characteristics of the failed material in front of a rod penetrating initially intact material. At first glance the results from the pre-damaged (thermally shocked) targets would suggest that the failed material in front of a rod penetrating initially intact SiC is significantly less damaged than the thermally shocked material studied here. However, this doesn't seem plausible to us. So we have begun looking for a more plausible explanation for the unexpectedly large difference in the penetration resistance exhibited by the pre-impact intact and the pre-damaged materials studied. Recent but preliminary, numerical simulations suggest that the apparent "weakness" of the pre-damaged material may be the consequence of the fact that the *entire target* was weakened by the thermal treatment. In penetrating an initially intact target, a more spatially limited region near the rod is expected to be damaged/weakened based on the results of these numerical simulations. That is, the level of damage *and the spatial extent of that damage* are both important to the resistance of a target to penetration, and these characteristics are not independent of one another.

Admittedly, the results of these experiments only indirectly, primarily through penetration velocity, address the nature of the material in front of a penetrating rod. Although there has been an effort to quantify the constitutive response of the failed material [9], there have not been any direct measurements of its spatial extent. The work in Refs. [8-9] were the first application of a new experimental technique to quantify the strength of failed SiC under confinement. This technique has since evolved and been improved, and applied to glass [10-12]. Thus, we believe work on glass, such as ballistic experiments, e.g., [1], as well as numerical simulations using various constitutive models [21-22], are complementary to the work presented here.

5.0 Acknowledgements

The authors would like to thank Dr. Robert Mason of Southwest Research Institute for his is support in statistical analyses of the experimental data. The authors also thank Dr. Volker Hohler and Dr. Mathias Wickert of Ernst-Mach-Institut for their technical and administrative support.

6.0 References

1. Behner Th, Anderson CE Jr, Orphal DL, Hohler V, Moll M, and Templeton, DW. Penetration and failure of lead and borosilicate glass against rod impact. *Int. J. Impact Engng.*, 2007, accepted for publication.

2. Holmquist TJ and Johnson GR. Response of silicon carbide to high velocity impact. *J. Appl. Phys.*, 2002, **91**(9): 5858-5866.

3. Kloop RW and Shockey DA. Strength behavior of granulated silicon carbide at high strain rates and confining pressures. *J. Appl. Phys*., 1991, **70**(12): 7318-7326.

4. Holmquist TJ and Johnson GR. Ceramic dwell and interface defeat. *Ceramic Transactions, Ceramic Armor Materials by Design*, (J. McCauley, *et al*., Eds.), 2002, **134**: 485-498.

5. Holmquist TJ Johnson GR. Modeling prestressed ceramic and its effects on ballistic performance. *Int. J. Impact Engng*., 2005, **31**: 113-127.

6. Holmquist TJ and Johnson GR. Characterization and evaluation of silicon carbide to high velocity impact. *J. Appl. Phys.*, 2005, **97**(09): 093502/1-12.

7. Anderson CE Jr. A review of computational armor ceramics modeling. ***Advances in Ceramic Armor II***, *A Collection of Papers Presented at the 30th Int. Conf. & Exp. on Advanced Ceramics and Composites* (L P Franks, Ed.), **27**(7): 1-18, John Wiley & Sons, Inc., NJ., 2006.

8. Dannemann KA, Nicholls AE,Chocron S, Walker JD, and Anderson CE Jr. Compression testing and response of SiC-N ceramics: intact, damaged and powder. ***Advances in Ceramic Armor***, *Proc. 29th Int. Conf. Advanced Ceramics & Composites* (J. J. Swab, Ed.), 2005, **26**(7): 109-116, American Ceramics Society, Westerville, OH.

9. Chocron S, Dannemann KA, Nicholls AE, Walker JD, and Anderson CE Jr. A constitutive model for damaged and powder silicon carbide. ***Advances in Ceramic Armor***, *Proc. 29th Int. Conf. Advanced Ceramics & Composites* (J. J. Swab, Ed.), 2005, **26**(7): 35-42, American Ceramics Society, Westerville, OH.

10. Chocron S, Dannemann KA, Walker JD, Nicholls AE, and Anderson CE Jr. Constitutive model for damaged borosilicate glass under confinement. *J. Am Cer. Soc.*, 2007, **90**(8): 2549-2555.

11. Chocron S, Dannemann KA, Walker JD, Nicholls AE, and Anderson CE Jr. Analytic model of the confined compression test used to characterize brittle materials. *J. Appl. Mech.*, 2007, accepted for publication.

12. Dannemann KA, Chocron S, Nicholls AE, and Anderson CE Jr. Compressive damage development in confined borosilicate glass. *J. Mat. Sci. & Engng. A*, 2007, accepted for publication.

13. Behner Th, Orphal DL, Hohler V, Anderson Jr CE, Mason RL, Templeton DW. Hypervelocity penetration of gold rods into SiC–N for impact velocities from 2.0 to 6.2 km/s. *Int J Impact Eng*, 2006, **33**(1-12): 68-79.

14. Dandekar D. Spall strength of silicon carbide under normal and simultaneous compression-shear shock wave loading. *Int. J. Appl. Ceram. Technol.*, 2004, **1**(3): 261-268.

15. Holmquist, TJ. Personal communication.

16. Tate A. Long rod penetration models—Part II. Extensions to the hydrodynamic theory of penetration. *Int. J. Engng. Sci.*, 1986, **28**(9): 599-612.

17. Holmquist TJ, Anderson CE Jr, and Behner T. Design, analysis and testing of an unconfined ceramic target to induce dwell. *Proc. 22nd Int. Symp. Ballistics*, 2005, **2**: 860-868, DES*tech* Publications, Inc., Lancaster, PA.

18. Anderson CE Jr and Chocron S. A constitutive model for *in-situ* comminuted silicon carbide. *32nd Int. Conf. & Expos. on Advanced Ceramics and Composites,* The American Ceramics Society, Jan. 27 – Feb 1, Daytona Beach, FL, 2008.

19. Holmquist TJ and Johnson GR. The ballistic response of silicon carbide powder. *32nd Int. Conf. & Expos. on Advanced Ceramics and Composites*, The American Ceramics Society, Jan. 27 – Feb 1, Daytona Beach, FL, 2008.

20. Orphal DL and Anderson CE Jr. The dependence of penetration velocity on impact velocity. *Int. J. Impact Engng*., 2006, **33**(1-12): 546-554.

21. Chocron S, Anderson CE Jr, and Nicholls AE. Constitutive model for borosilicate glass and application to long-rod penetration. *23rd Int. Symp. Ballistics*, **2**, pp. 1073-1081, Gráficas Couche, Madrid, Spain 2007.

22. Johnson GR and Holmquist TJ. Some preliminary constitutive models for glass subjected to high-velocity impact. *32nd Int. Conf. & Expos. on Advanced Ceramics and Composites,* The American Ceramics Society, Jan. 27 – Feb 1, Daytona Beach, FL, 2008.

Appendix A: Position-Time Data

Table A1. Position-Time Data for Experiments

C			PD			CP		
	t after imp [µs]	pen depth [mm]		t after imp [µs]	pen depth [mm]		t after imp [µs]	pen depth [mm]
11046			11065	24.96	25.13	11049	44.96	20.58
	26.47	3.60		16.99	16.19		30.01	16.09
	16.58	2.41		10.37	7.47		20.78	11.24
	5.75	-0.18		3.37	1.02		8.56	3.36
	0.00	-3.18		0.00	-3.18		0.00	-3.18
11048	65.13	14.93	11068	26.43	35.48	11053	38.76	32.60
	49.87	13.49		20.44	26.48		28.41	23.50
	35.69	11.73		15.00	18.22		18.91	15.03
	19.33	7.27		0.00	0.00		8.01	4.85
	0.00	-3.18		0.00	-3.18		0.00	-3.18
11050	51.27	22.47	11069	21.50	29.47	11057	26.66	30.26
	31.21	14.90		15.60	20.38		19.37	21.26
	21.95	10.46		11.73	14.57		12.83	12.70
	10.64	4.35		4.35	3.55		4.70	2.48
	0.00	-3.18		0.00	-3.18		0.00	-3.18
11052	48.21	27.17	11071	21.03	31.66	11067	19.34	30.57
	35.60	23.49		15.40	21.82		13.83	21.74
	24.39	16.29		10.88	14.92		10.11	15.56
	11.11	6.07		4.60	4.60		4.06	5.17
	0.00	-3.18		0.00	-3.18		0.00	-1.70
11056	31.99	32.29	11074	18.33	30.34	11073	18.09	33.82
	23.50	23.46		13.65	22.73		14.62	26.95
	16.04	13.97		10.27	15.60		11.30	20.40
	6.76	5.68		3.89	4.38		4.85	7.36
	0.00	-3.18		0.00	-3.18		0.00	-2.00
11058	33.35	30.67				11077	28.82	35.65
	25.33	22.61					22.02	26.86
	17.99	16.17		C			15.90	18.78
	8.57	6.58		t after imp [µs]	pen depth [mm]		7.34	7.41
	0.00	-3.18					0.00	-3.18
11064	25.59	28.52	11072	18.75	32.64			
	17.79	18.36		14.26	24.53			
	11.39	10.60		10.76	18.21			
	4.40	2.63		4.53	6.33			
	0.00	-3.18		0.00	-3.18			
11066	23.40	31.64	11075	20.77	34.23			
	17.92	23.04		14.92	23.91			
	12.11	14.77		11.37	17.35			
	5.03	4.56		4.60	5.16			
	0.00	-3.18		0.00	-3.18			
11070	20.98	32.88	11076	25.47	31.50			
	15.58	23.91		18.75	22.39			
	11.08	16.14		13.99	16.97			
	4.73	4.87		6.09	5.31			
	0.00	-3.18		0.00	-3.18			

Appendix B: X-Ray Shadowgraphs

The appendix contains the X-ray shadowgraphs for each of the experiments. The X-ray shadowgraphs are in original grayscale (not inverted) to enhance visibility of the eroding rod.

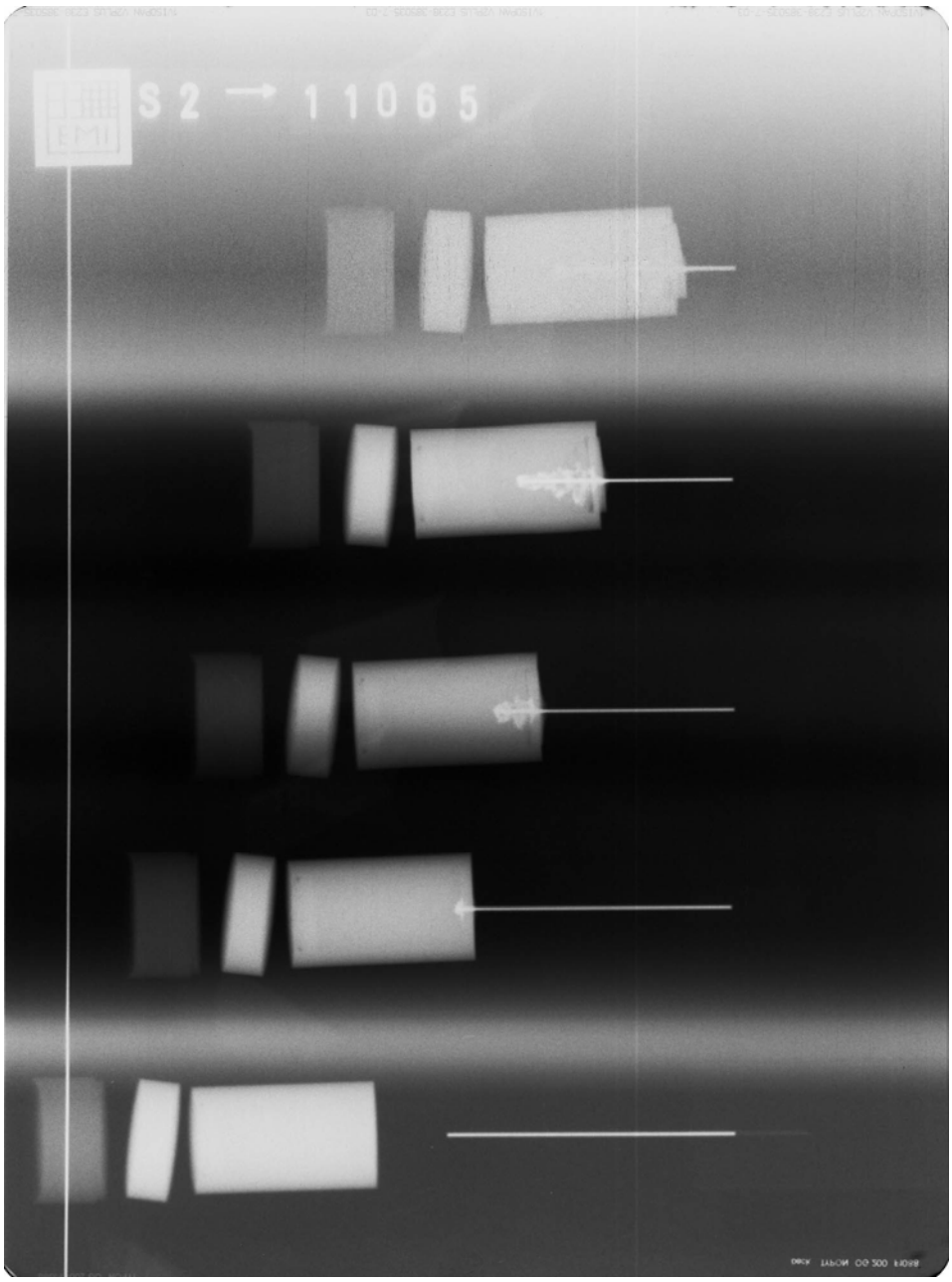

Figure B-1. X-ray shadowgraph for Expt. 11065: PD-SiC, v_P = 2209 m/s

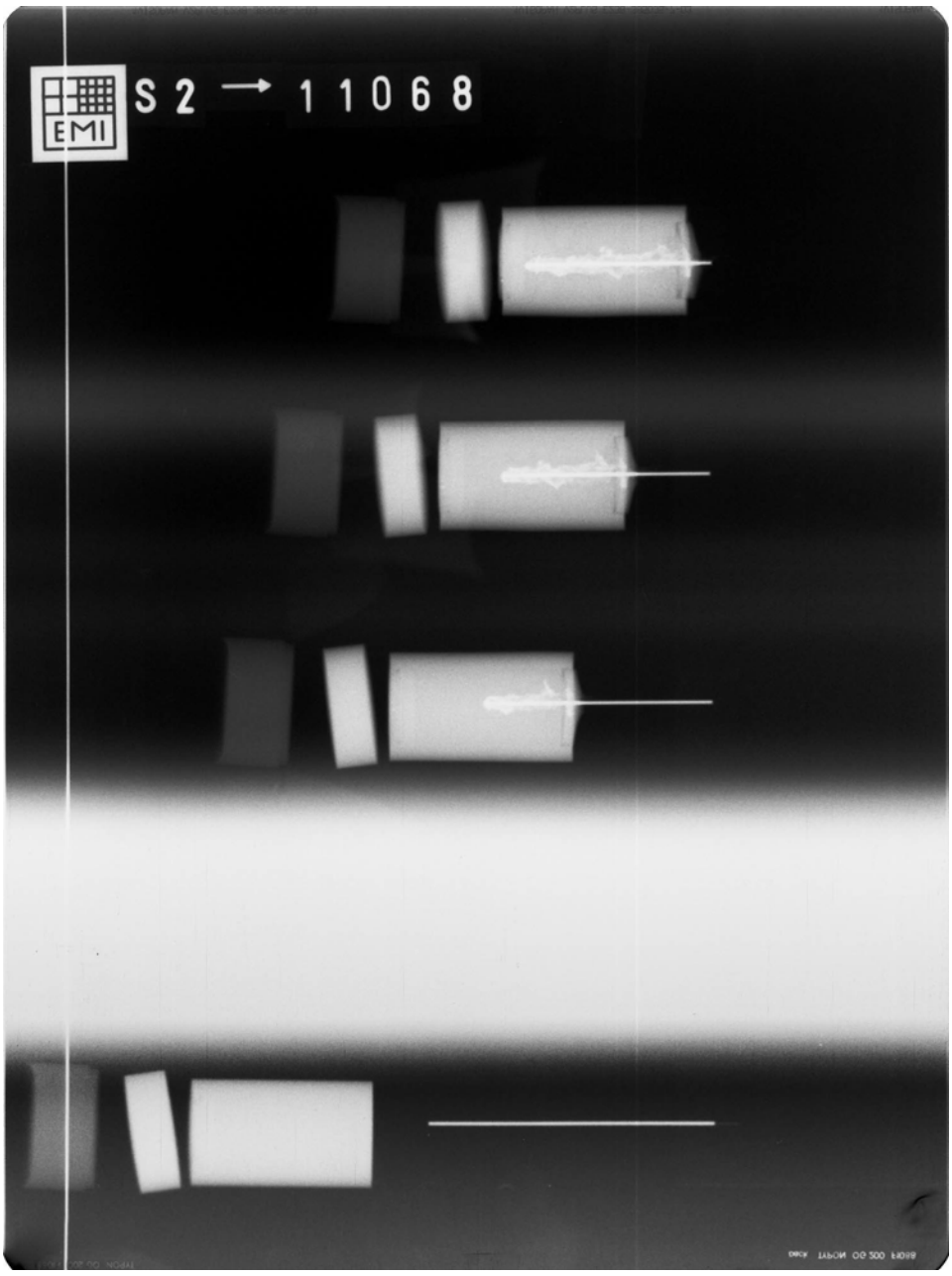

Figure B-2. X-ray shadowgraph for Expt. 11068: PD-SiC, v_p = 2414 m/s

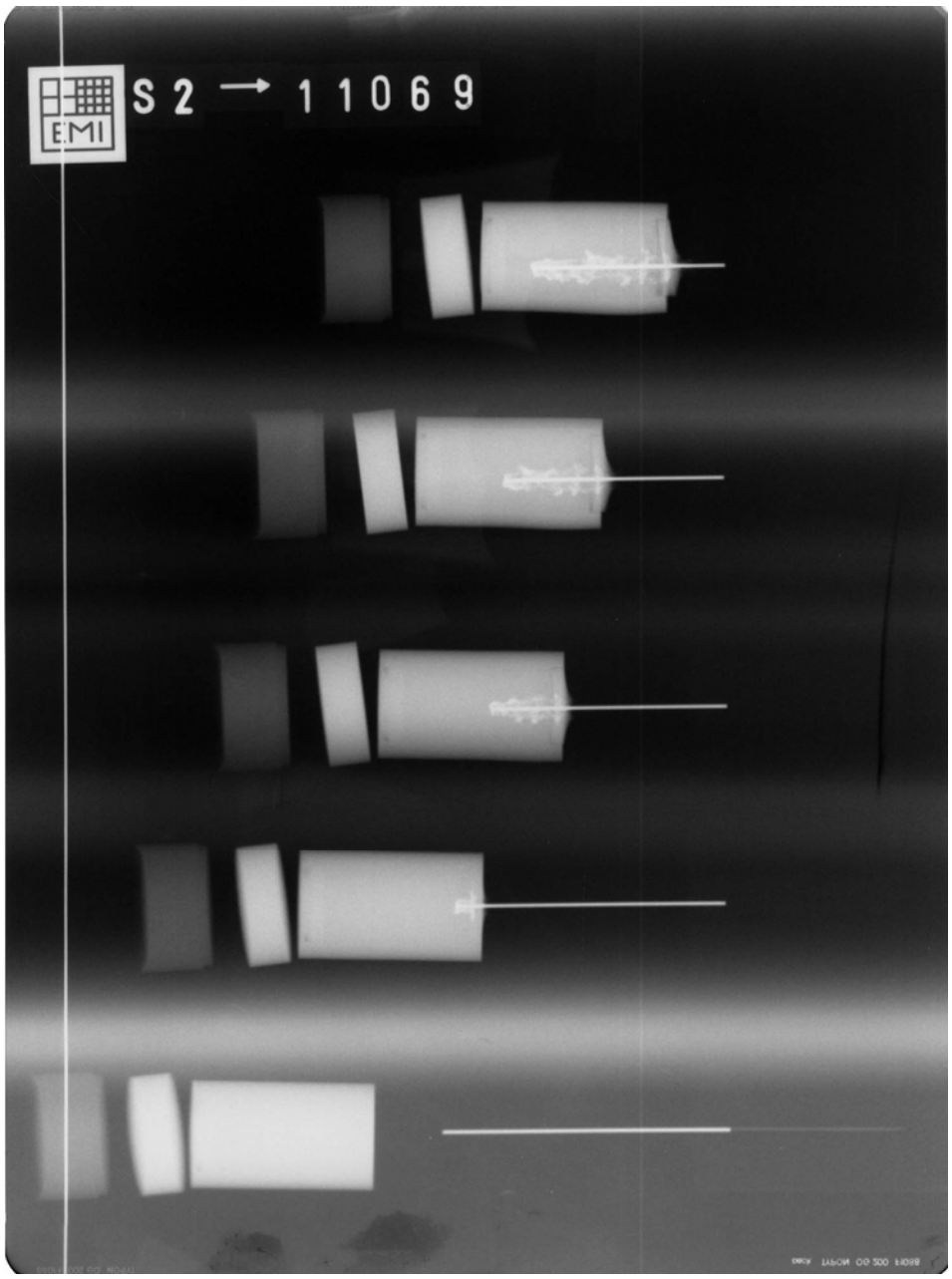

Figure B-3. X-ray shadowgraph for Expt. 11069: PD-SiC, v_P = 2614 m/s

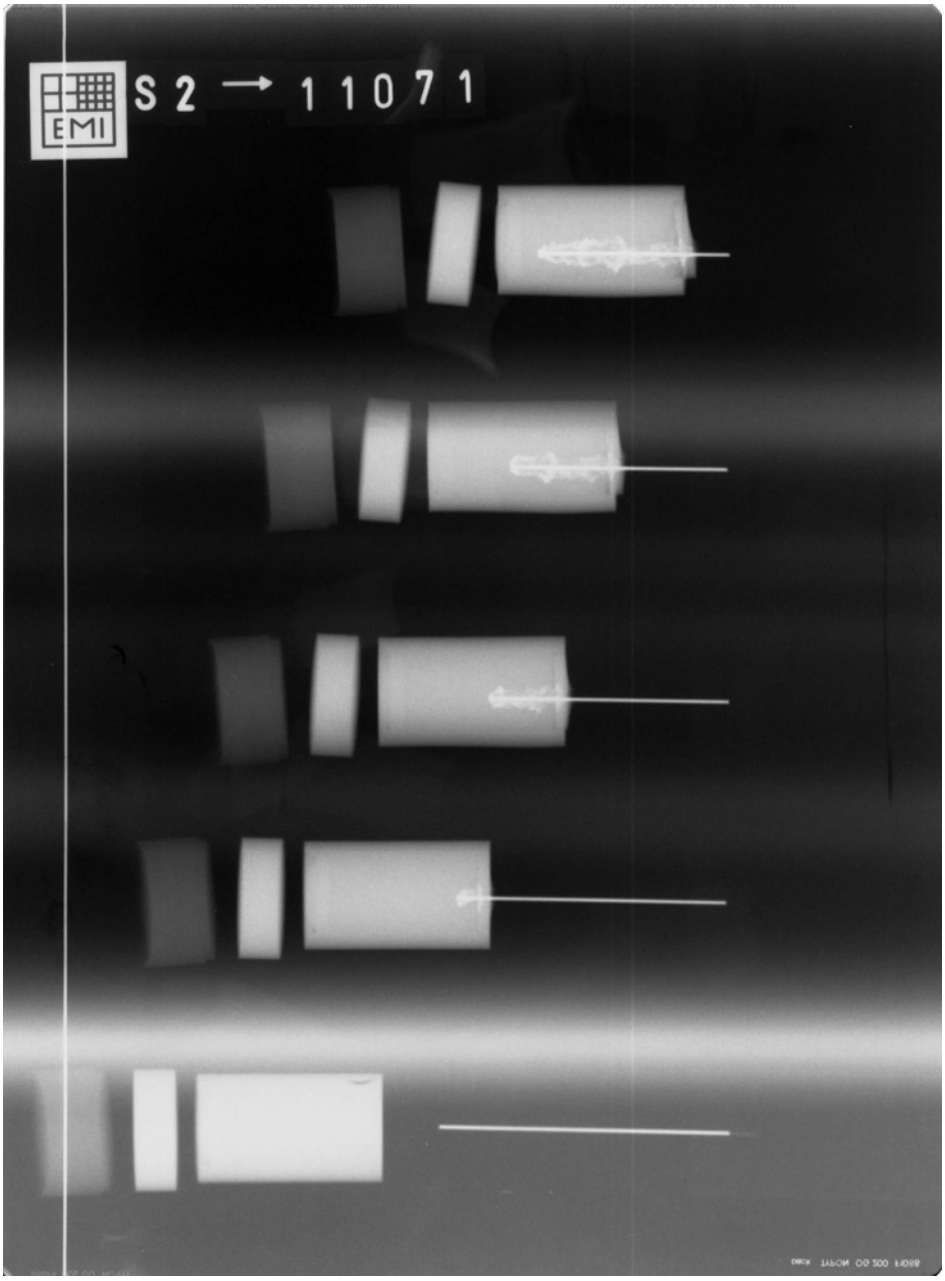

Figure B-4. X-ray shadowgraph for Expt. 11071: PD-SiC, v_P = 2816 m/s

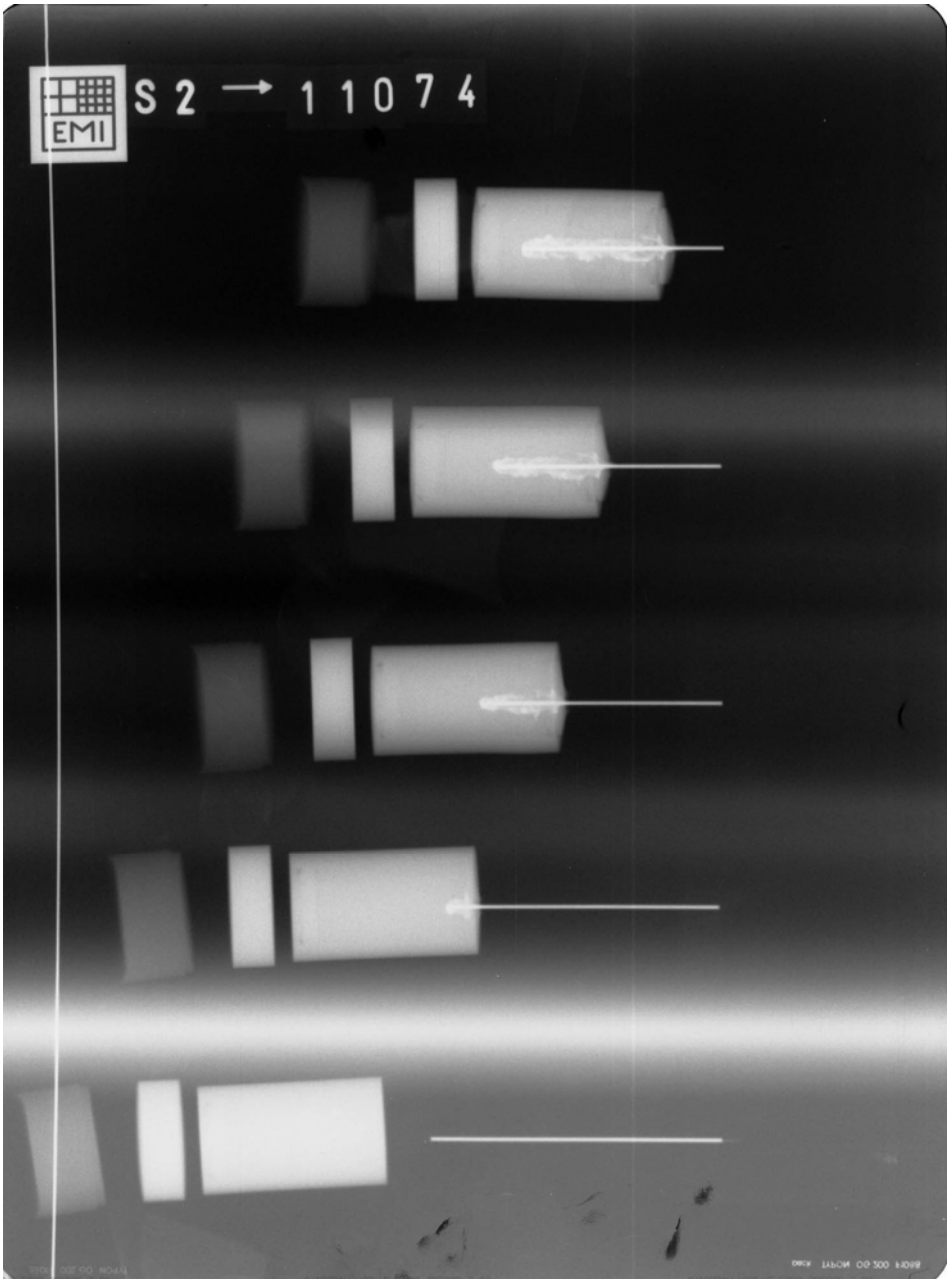

Figure B-5. X-ray shadowgraph for Expt. 11074: PD-SiC, v_P = 3037 m/s

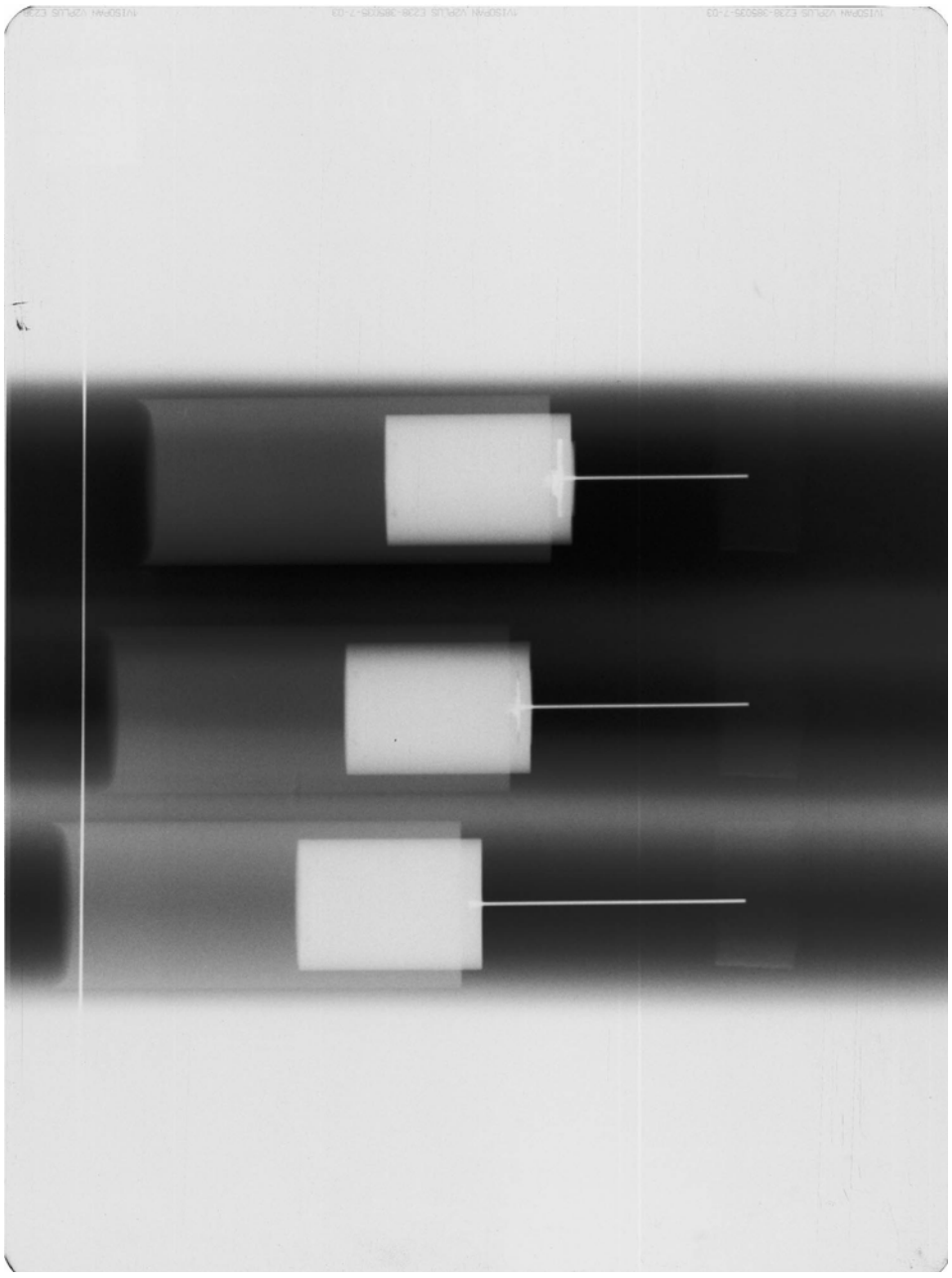

Figure B-6: X-ray shadowgraph for Expt. 11046: C-SiC, v_P = 1039 m/s

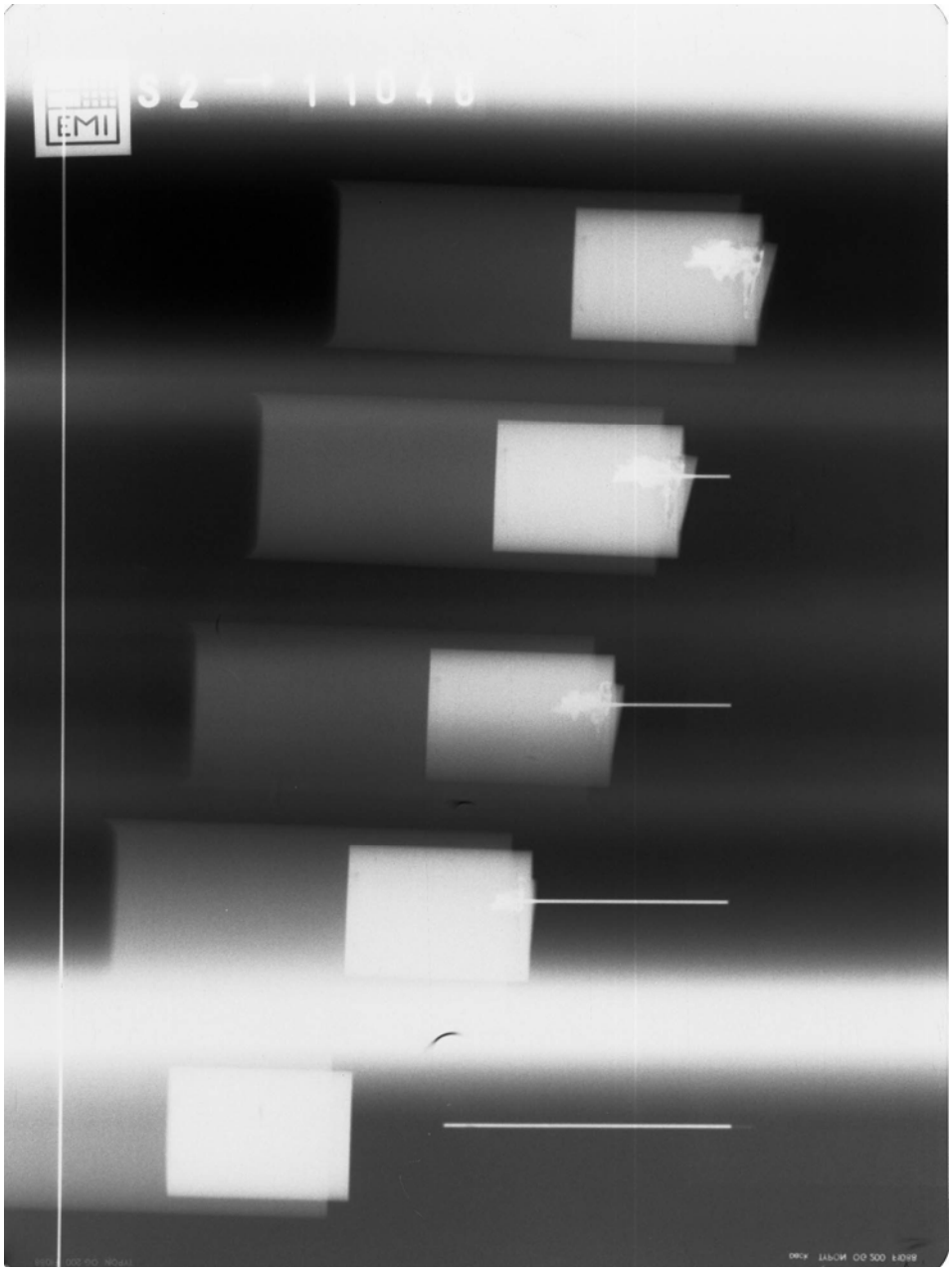

Figure B-7. X-ray shadowgraph for Expt. 11048: C-SiC, v_p = 1170 m/s

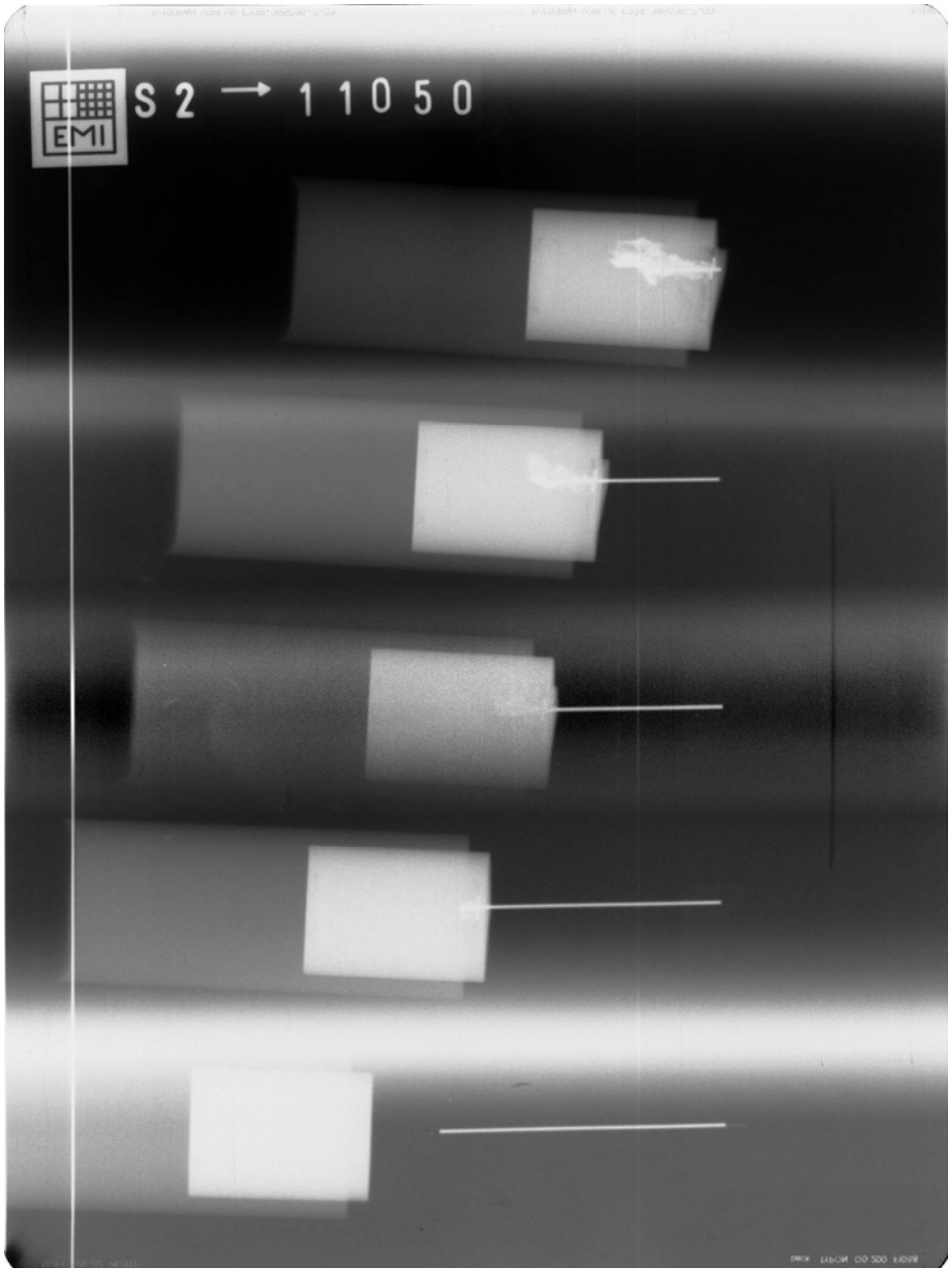

Figure B-8. X-ray shadowgraph for Expt. 11050: C-SiC, v_P = 1340 m/s

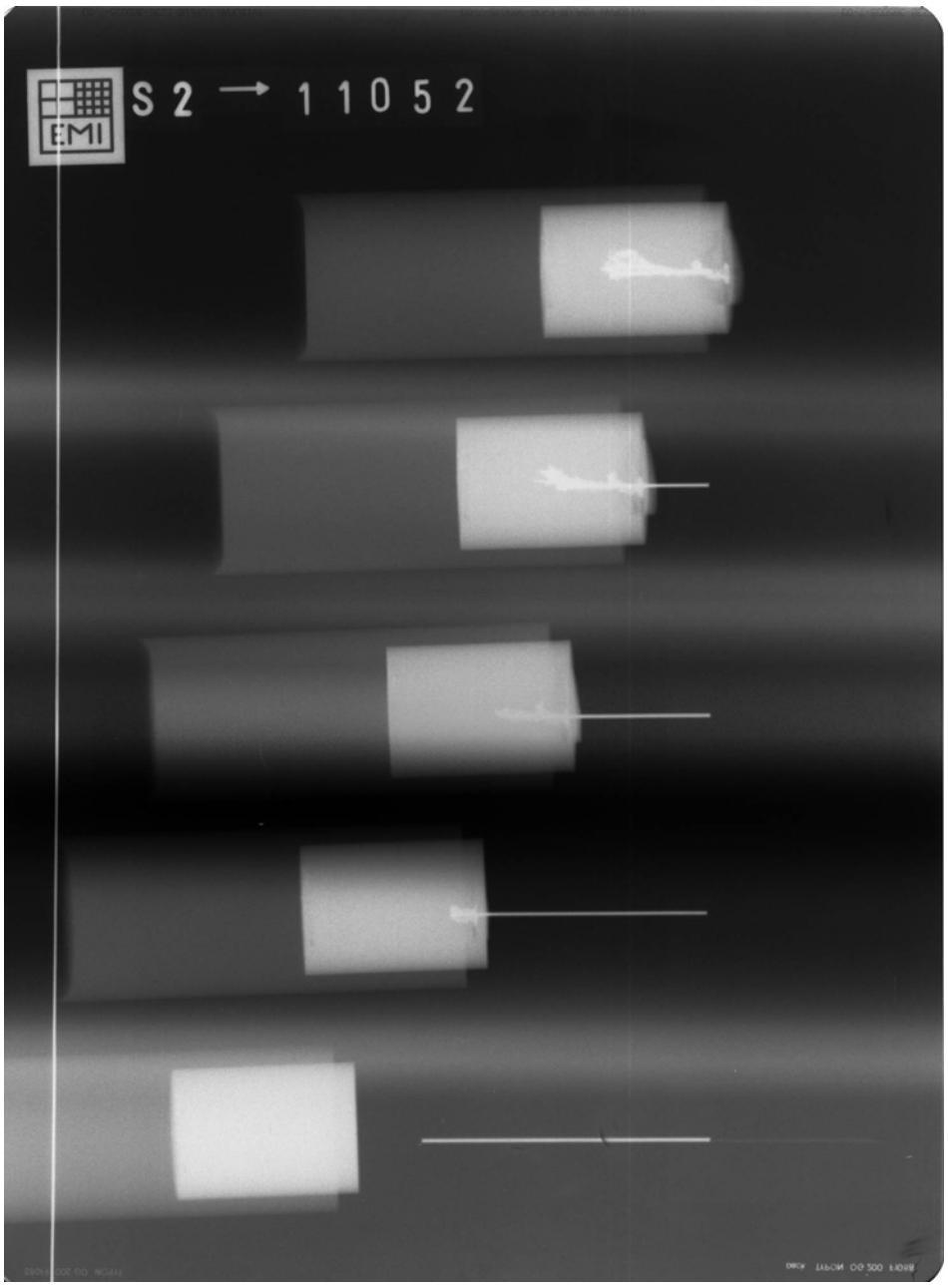

Figure B-9. X-ray shadowgraph for Expt. 11052: C-SiC, v_P = 1535 m/s

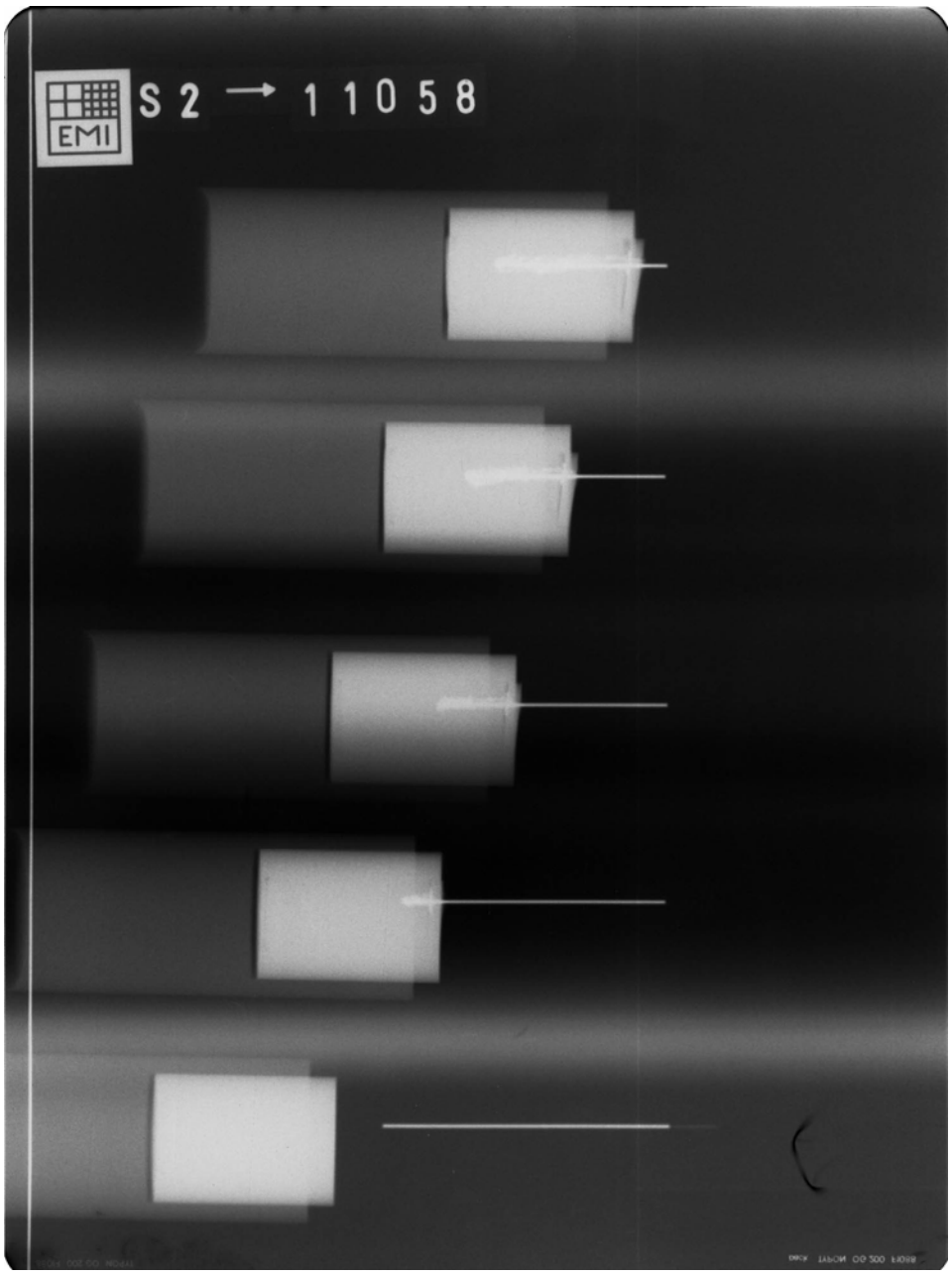

Figure B-10. X-ray shadowgraph for Expt. 11058: C-SiC, v_P = 1874 m/s

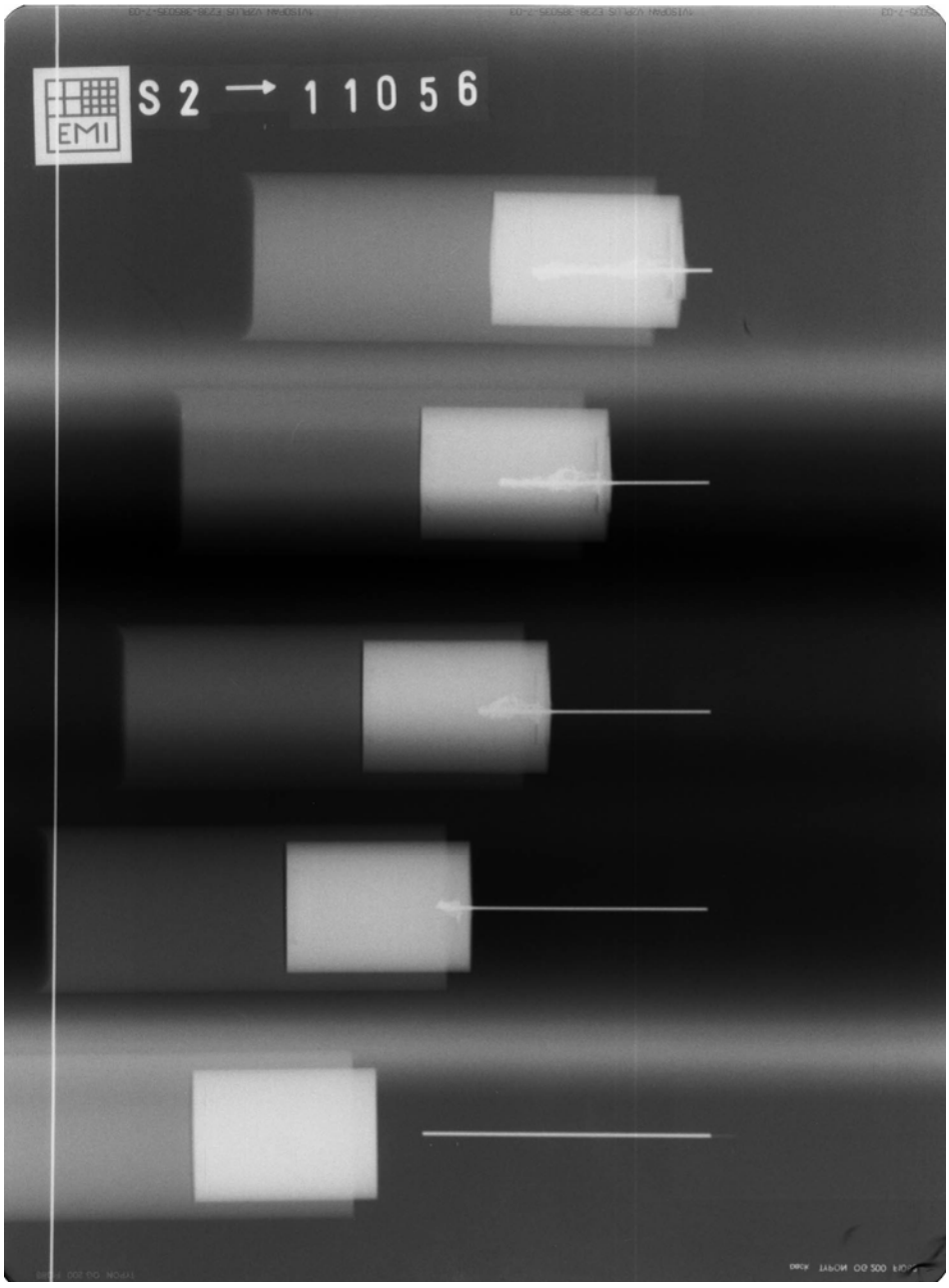

Figure B-11. X-ray shadowgraph for Expt. 11056: C-SiC, v_P = 1956 m/s

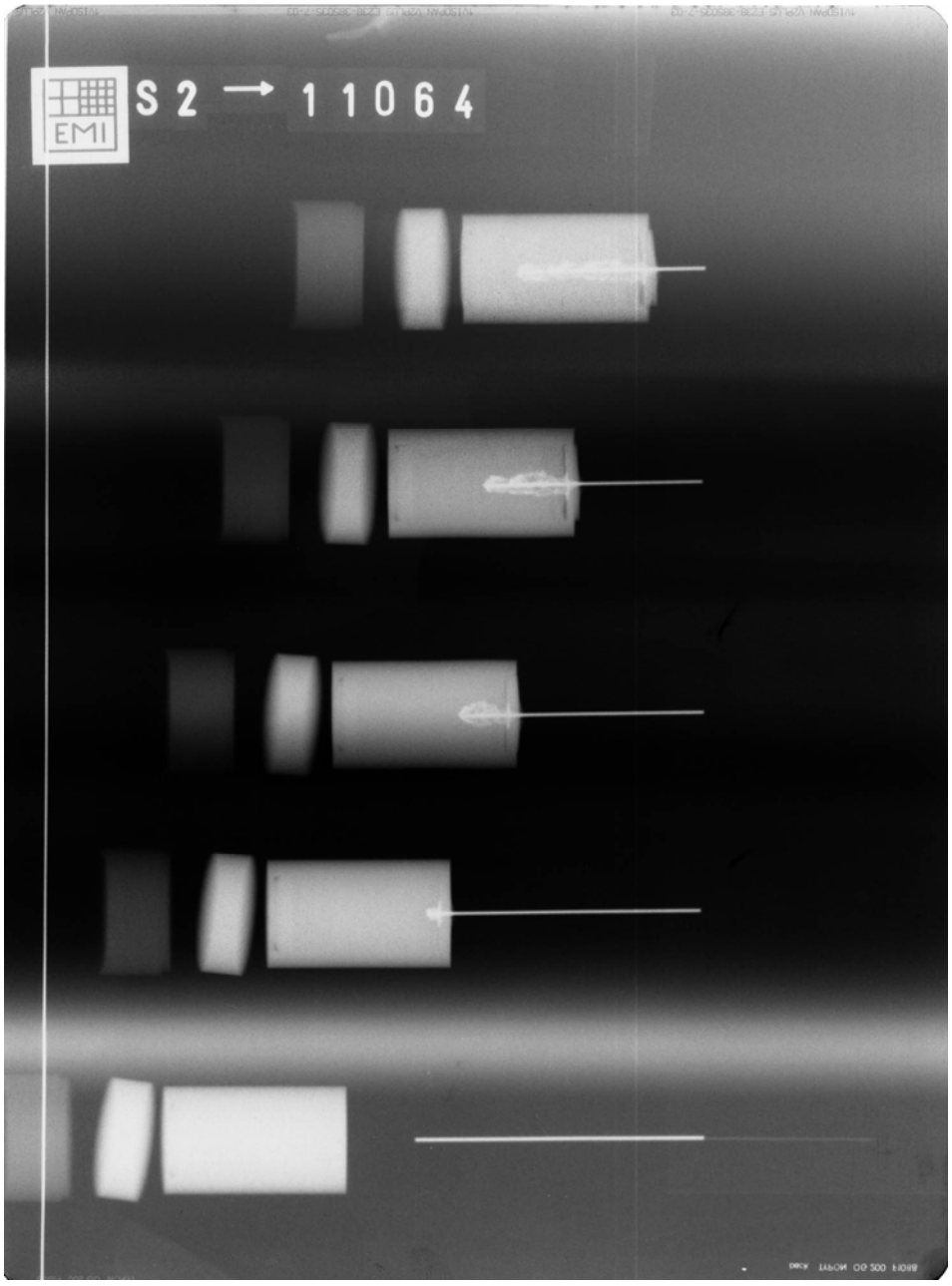

Figure B-12. X-ray shadowgraph for Expt. 11064: C-SiC, v_P = 2201 m/s

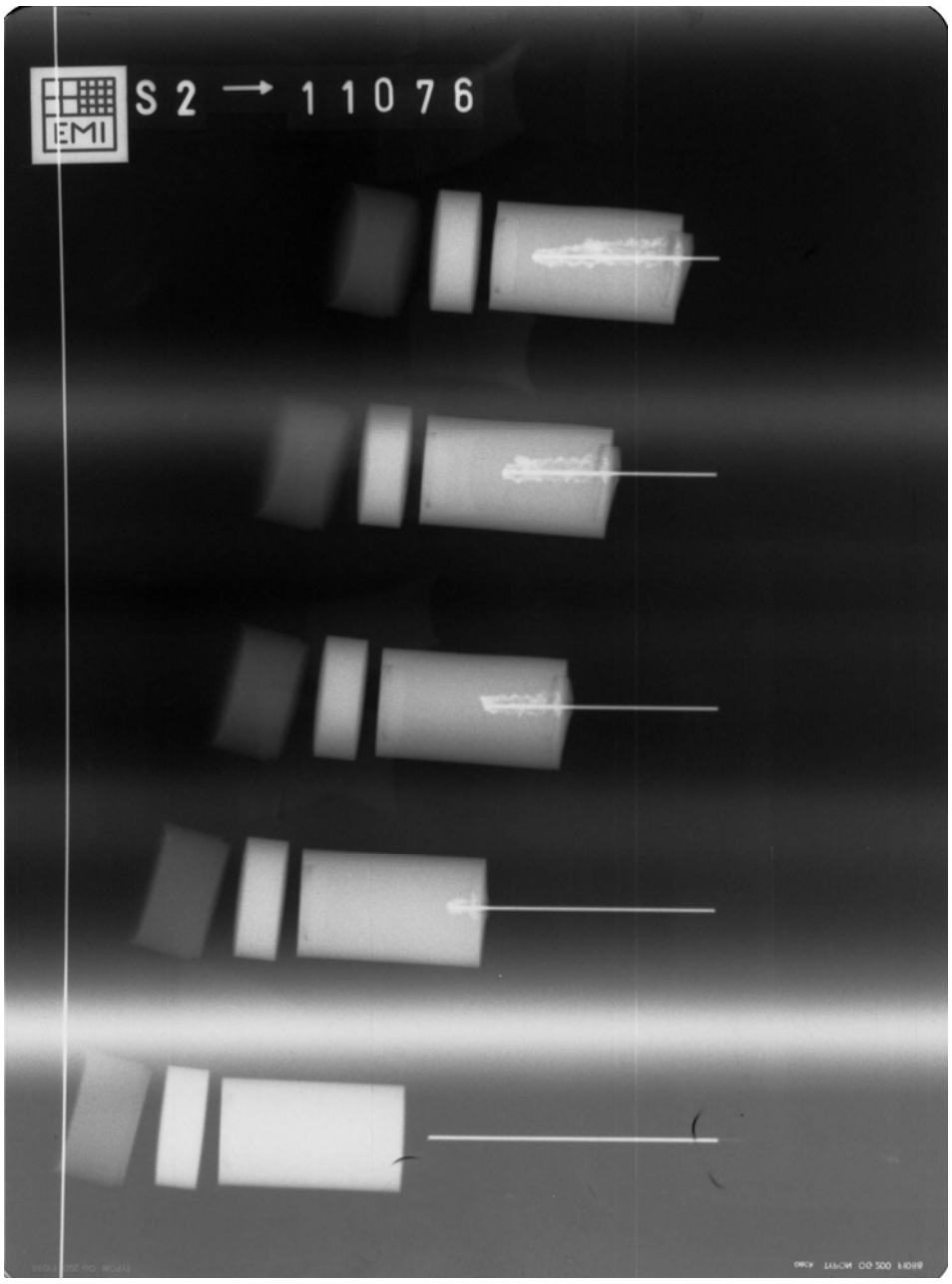

Figure B-13. X-ray shadowgraph for Expt. 11076: C-SiC, v_P = 2367 m/s

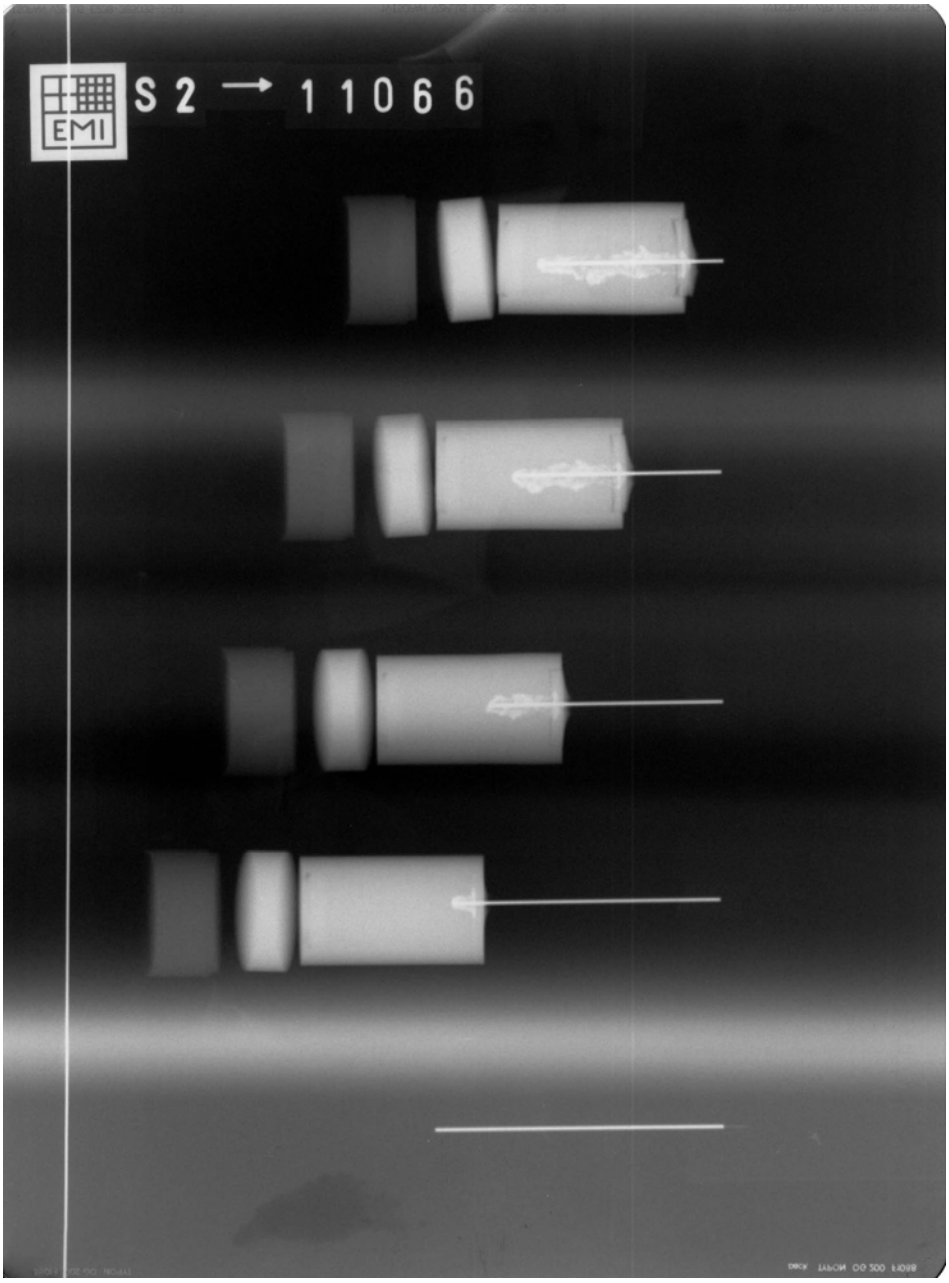

Figure B-14. X-ray shadowgraph for Expt. 11066: C-SiC, v_P = 2585 m/s

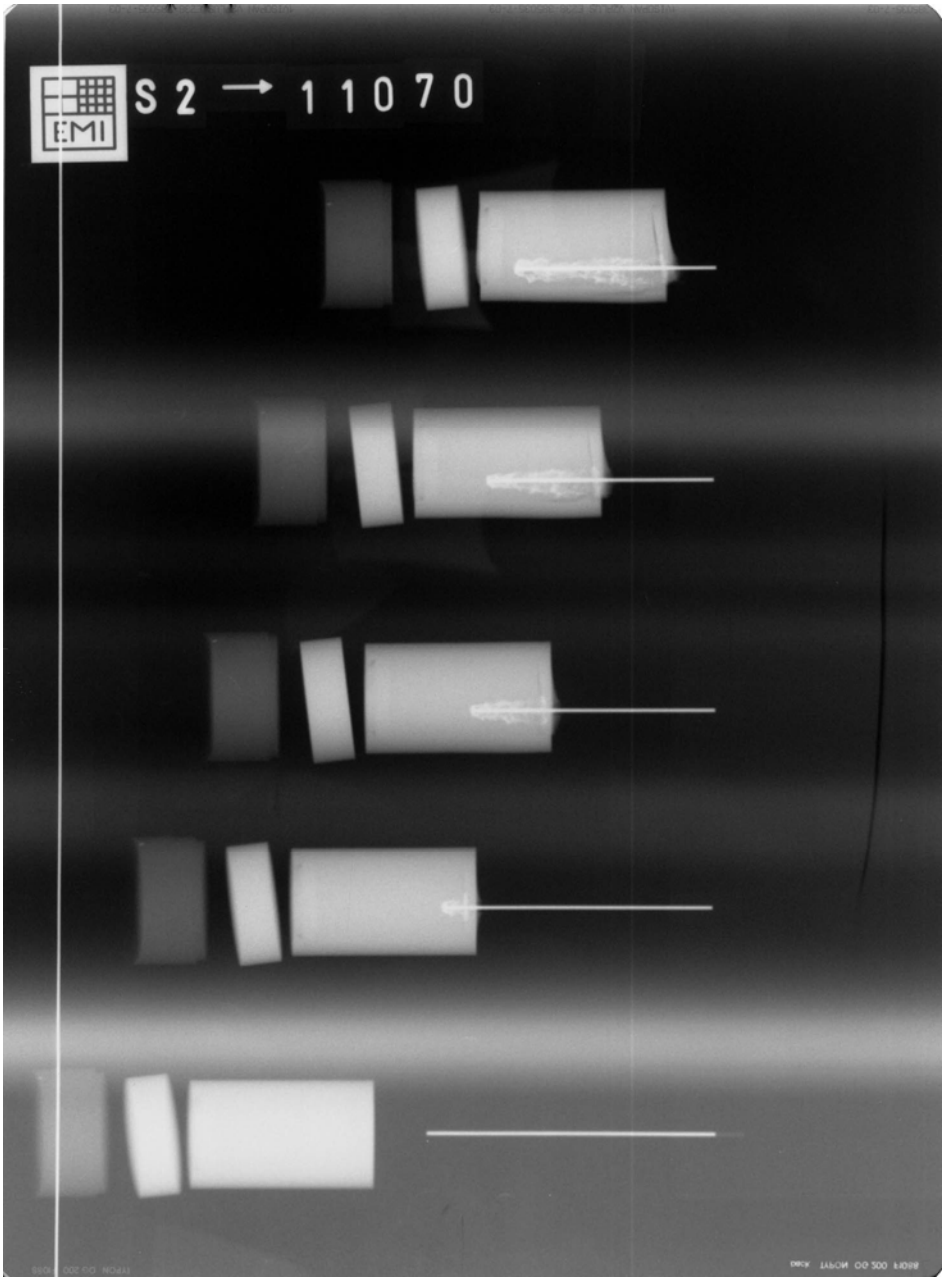

Figure B-15. X-ray shadowgraph for Expt. 11070: C-SiC, v_P = 2765 m/s

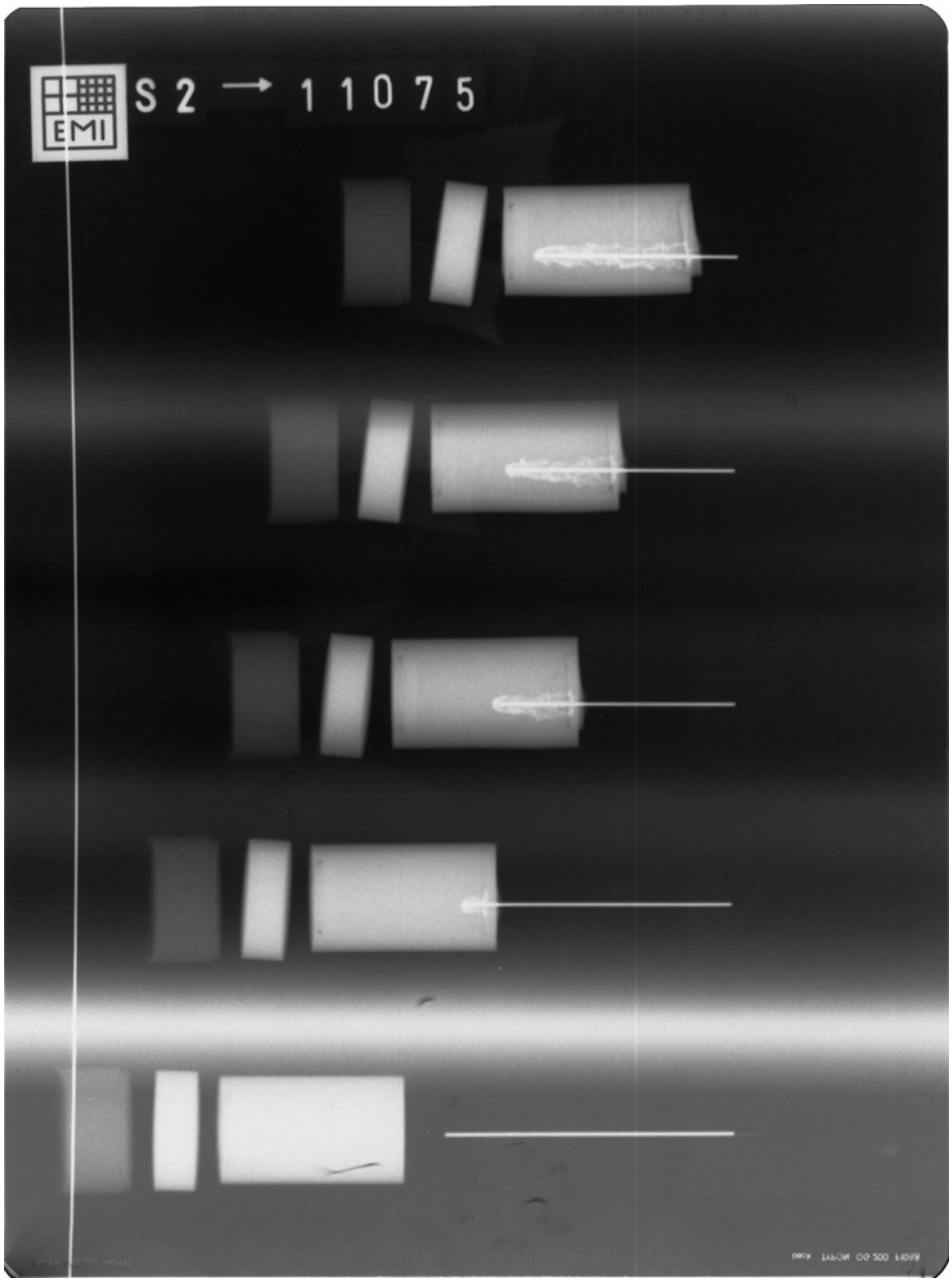

Figure B-16. X-ray shadowgraph for Expt. 11075: C-SiC, v_P = 2835 m/s

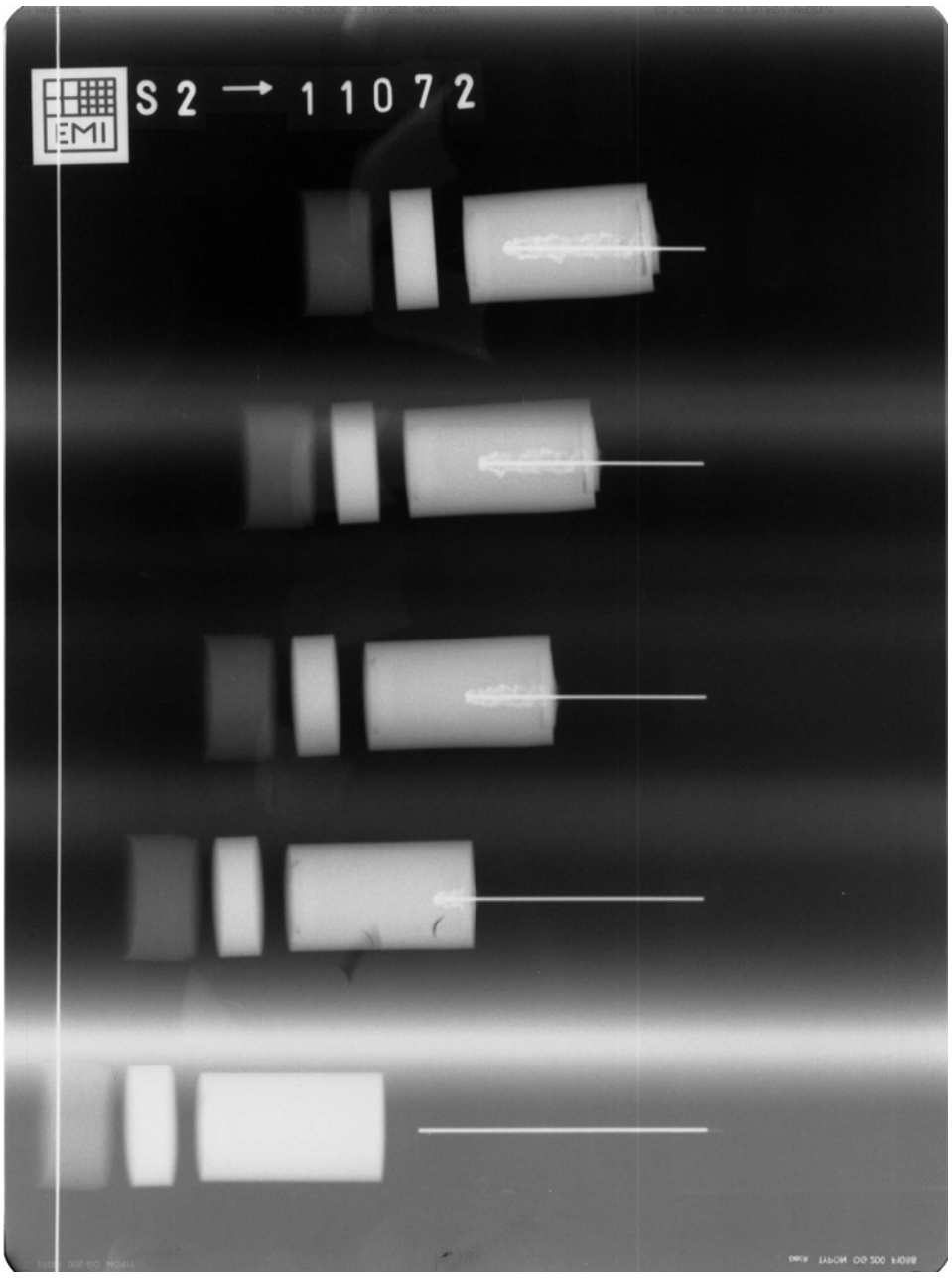

Figure B-17. X-ray shadowgraph for Expt. 11072: C-SiC, v_P = 3060 m/s

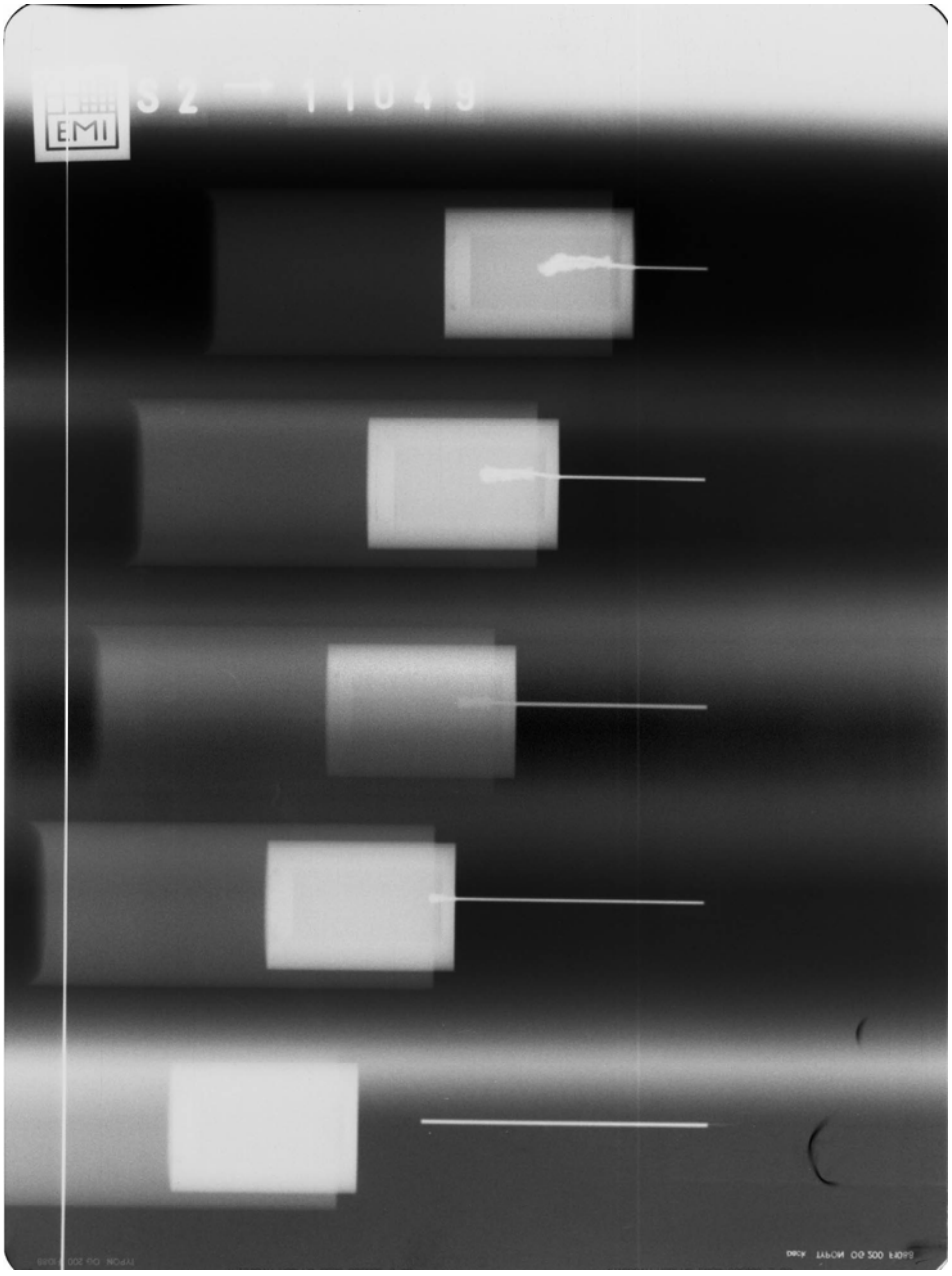

Figure B-18. X-ray shadowgraph for Expt. 11049: CP-SiC, v_P = 1172 m/s

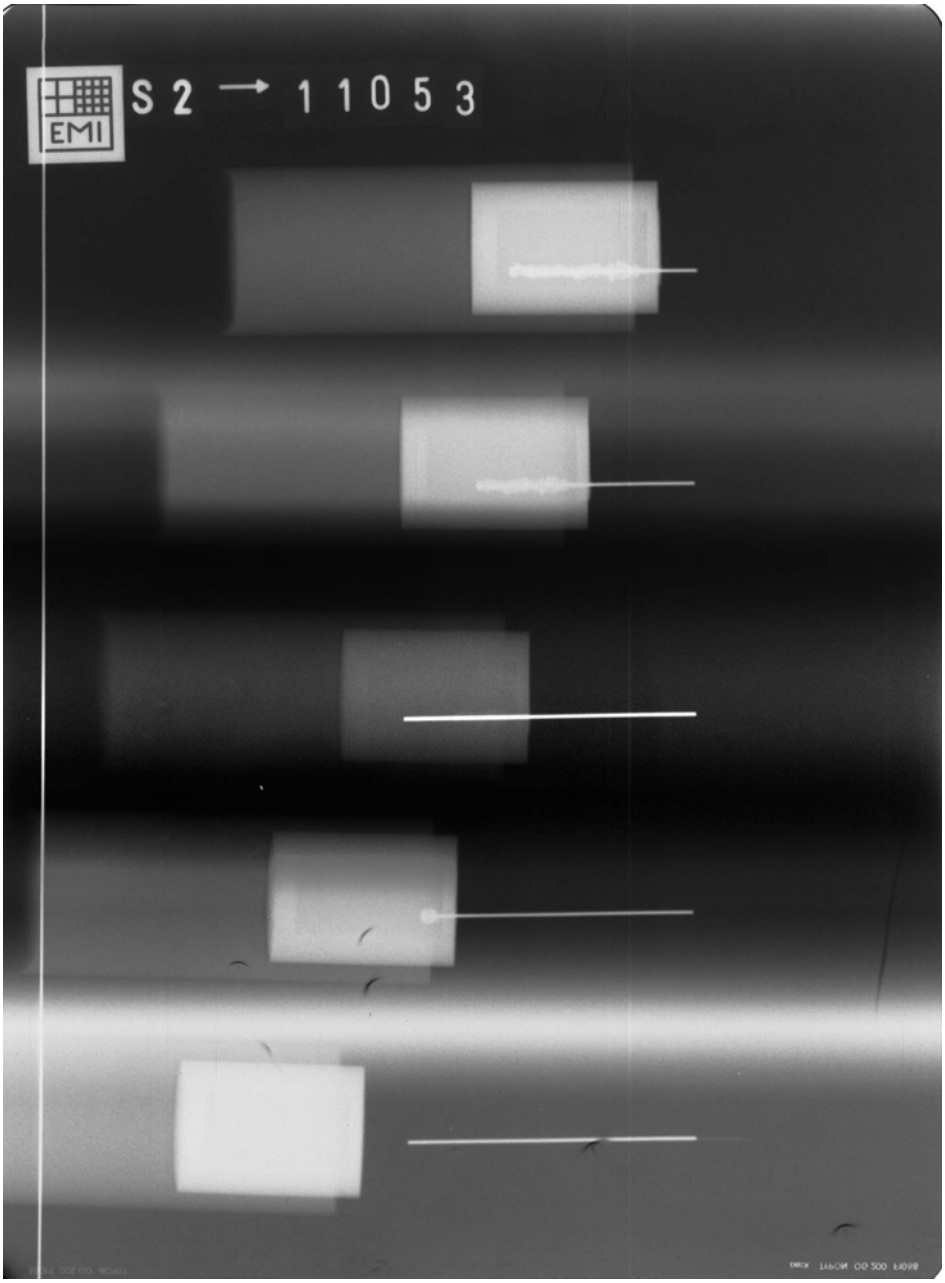

Figure B-19. X-ray shadowgraph for Expt. 11053: CP-SiC, v_P = 1574 m/s

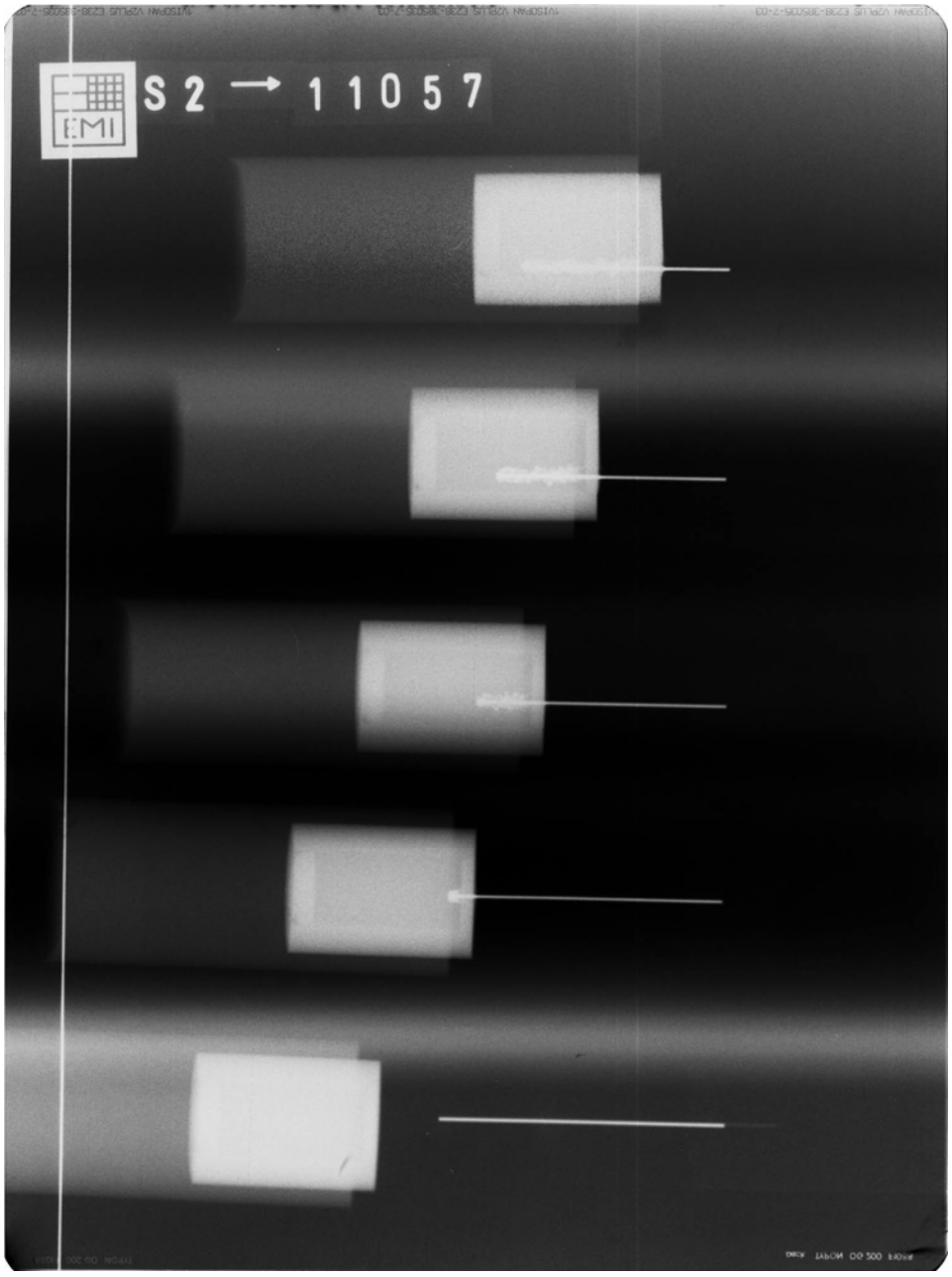

Figure B-20. X-ray shadowgraph for Expt. 11057: CP-SiC, v_P = 2006 m/s

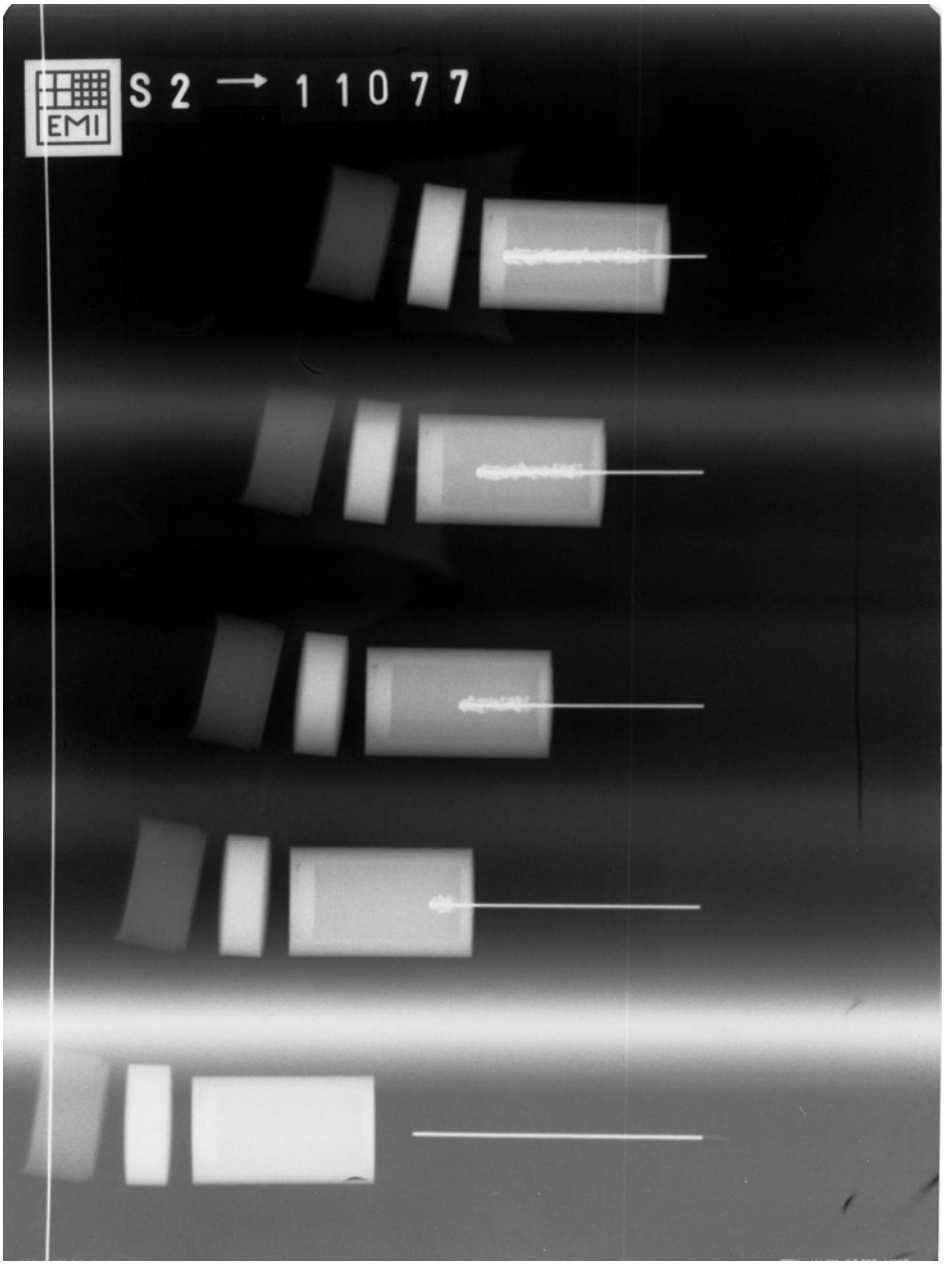

Figure B-21. X-ray shadowgraph for Expt. 11077: CP-SiC, v_P = 2088 m/s

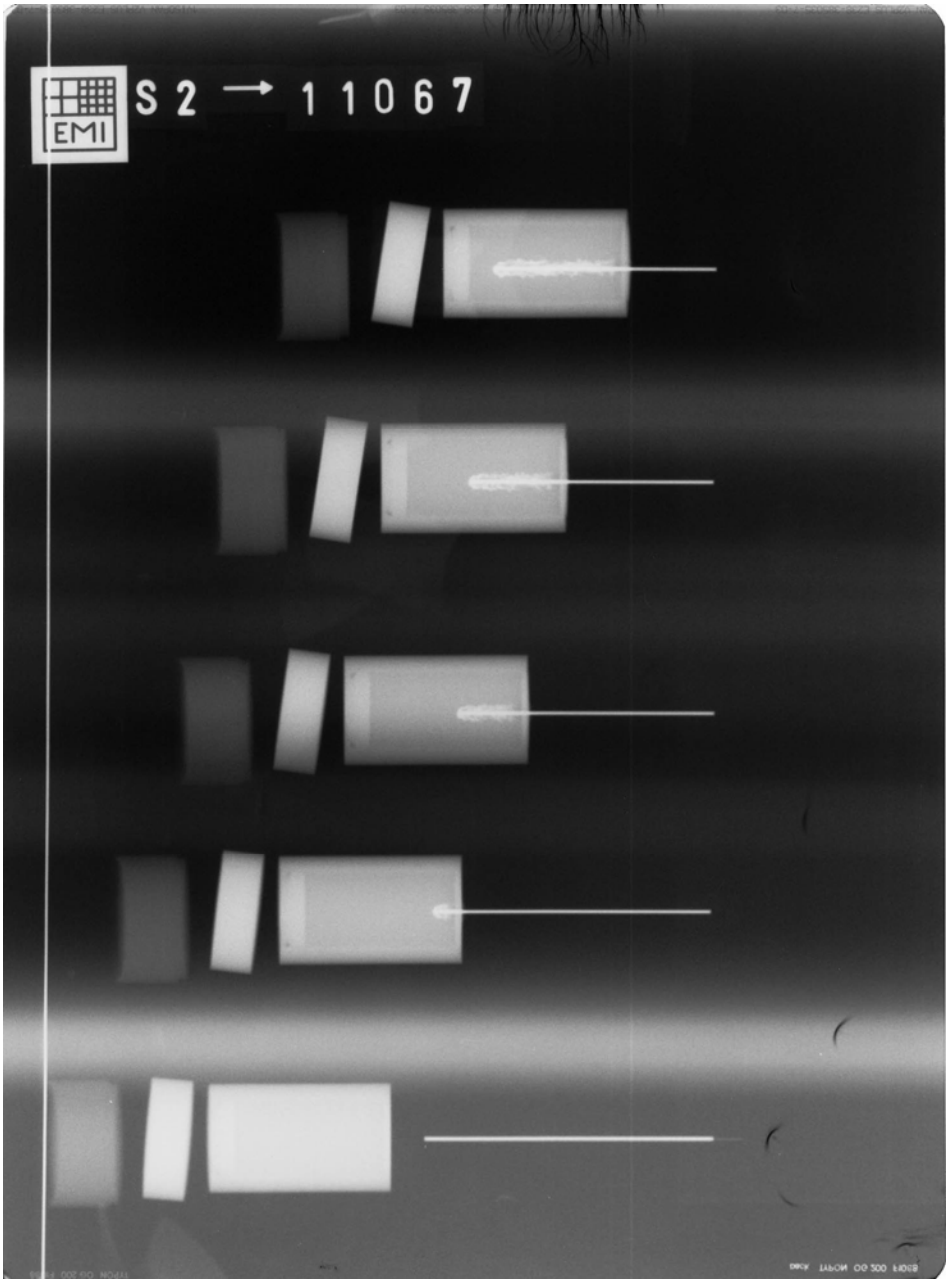

Figure B-22. X-ray shadowgraph for Expt. 11067: CP-SiC, v_P = 2535 m/s

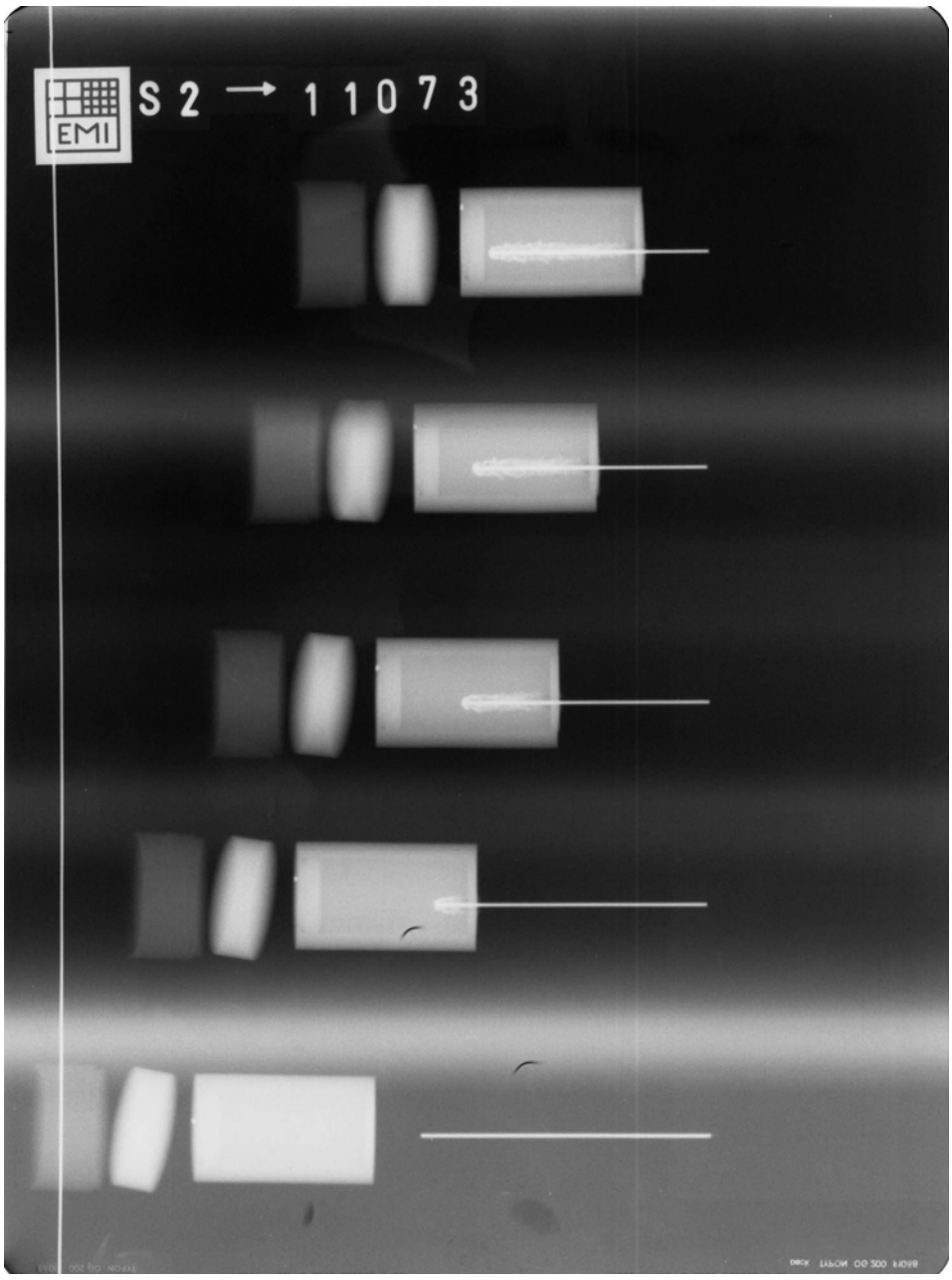

Figure B-23. X-ray shadowgraph for Expt. 11073: CP-SiC, v_P = 3010 m/s

Appendix C: Summary of Regression Fits

Linear least squares fit constants for u-v_p data for Au rods penetrating damaged SiC-N ("linear data" only).

Table C1. $u = a + bv_p$

SiC Material	Sample Size	*A*	*b*	r^2	*RMS*	*p*-Value
Predamaged	5	-0.3733	0.7240	0.8885	0.096	0.8488
Predamaged	4	-0.6578	0.8178	0.9950	0.025	0.2627
In-situ comminuted	8	-0.4864	0.7805	0.9788	0.053	0.6024
Compacted powder	5	-0.2760	0.7606	0.9985	0.019	0.9750

Table C2. $u = a + 0.7547v_p$

SiC Material	Sample Size	*A*	*b*	r^2	*RMS*
Predamaged	5	-0.4538	0.7547	0.8885	0.097
Predamaged	4	-0.4895	0.7547	0.9950	0.037
In-situ comminuted	8	-0.4231	0.7547	0.9788	0.055
Compacted powder	5	-0.2629	0.7547	0.9985	0.019

Notes:

1. The "Sample Size" indicates the number of observations included in the regression fit.
2. The "*a*" and "*b*" values indicate the estimated intercept and slope, respectively, for the regression equation.
3. The "r^2" value is the square of the correlation coefficient associated with the regression equation (i.e., the correlation coefficient between u and v_p).
4. The "*RMS*" is an estimate of the standard deviation of the residuals from the regression fit (i.e., root mean square error).
5. The "*p*-Value" is the probability associated with testing the hypothesis that the slope of the regression is different from 0.7547. Large *p*-values, i.e., greater than 0.05, indicate that the slope is not different from 0.7547.